Geologica Acta, Vol.9, Nºs 3-4, September-December 2011, 445-466
DOI: 10.1344/105.000001739
Available online at www.geologica-acta.com
geologica acta

Transient Cenozoic tectonic stages in the southern margin of the Caribbean plate: U-Th/He thermochronological constraints from Eocene plutonic rocks in the Santa Marta massif and Serranía de Jarara, northern Colombia

A. CARDONA [1][5] V. VALENCIA [2] M. WEBER [3] J. DUQUE [4] C. MONTES [1][5] G. OJEDA [6] P. REINERS [7] K. DOMANIK [8]
S. NICOLESCU [7] D. VILLAGOMEZ [9]

[1] **Smithsonian Tropical Research Institute.** Balboa, Ancón, Panamá

[2] **Earth and Environmental Science Department.** Washington State University, Pullman, Washington

[3] **Escuela de Geociencias y Medio Ambiente.** Universidad Nacional, Medellín, Colombia

[4] **Centro de Geociencias.** Universidad Autónoma de México, Querétaro, México

[5] **Corporación Geológica Ares.** Bogotá, Colombia

[6] **Instituto Colombiano del Petróleo-Ecopetrol.** Piedecuesta, Colombia

[7] **Department of Geosciences.** University of Arizona, Tucson, USA

[8] **Department of Planetary Sciences.** University of Arizona, Tucson, Arizona

[9] **Department of Earth Sciences.** University of Geneva, Switzerland

ABSTRACT

We use U-Th/(He) zircon and apatite thermochronology and Al in hornblende geobarometry from Eocene granitoids of the Sierra Nevada de Santa Marta and Guajira uplifted massifs in northern Colombia to elucidate the exhumation history of the northern South America continental margin and its bearing to Cenozoic Caribbean–South American plate interactions. Aluminium in hornblende geobarometry from the Eocene Santa Marta batholith yields pressures between 4.9±0.6kbar and 6.4±0.6kbar, which indicate that at least, 14.7-19.2km of unroofing took place since 56-50Ma in the northwestern Sierra Nevada de Santa Marta. In the Guajira Peninsula, calculated pressures for the Eocene Parashi stock are 2.3±0.6kbar and 3±0.6kbar. Stratigraphic considerations pertaining to Oligocene conglomerates from the Guajira area suggest that 6.9-9km of crust was lost between 50Ma and ca. 26Ma. U-Th/He zircon and apatite thermochronology from granitoids in the Sierra Nevada de Santa Marta shows the existence of major exhumation events in the Late Eocene (ca. 45-40Ma), Late Oligocene (ca. 25Ma) and Miocene (ca. 15Ma). The Guajira region records the Late Eocene to Early Oligocene (35-25Ma) event, but it lacks evidence for the Miocene exhumation phase. These differences reflect isolation of the Guajira region from the

Sierra Nevada de Santa Marta and the Andean chain due to extensive block rotation and transtensional tectonics that affected the region during post-Eocene times.
The post-Eocene events correlate in time with an increased convergence rate and the frontal approach of North and South America. It is suggested that the two major tectonic mechanisms that govern exhumation in these Caribbean massifs are: 1) subduction of the Caribbean plate, and 2) post Eocene changes in plate convergence obliquity and rates that caused the South American continental margin blocks to override the Caribbean plate. Temporal correlation with other Caribbean and Northern Andean events allows to resolve the regional Cenozoic plate tectonic reorganizations experienced by the South American, Caribbean and Pacific plates at a regional scale.

KEYWORDS | **U-Th/He thermochronology. Exhumation. Oblique convergence. Caribbean subduction.**

INTRODUCTION

Active margins characterized by multiple plate tectonic boundaries and surrounded by different oceanic plates are subjected to continuous and rapid changes in convergence relations and in the character of the accreted and/or subducted oceanic crust (Jarrard, 1986; Cross and Pilger, 1982; Cloos, 1993; Gutscher, 2002). Successive modifications of these plate configurations have magmatic, sedimentary, deformational and paleogeographic effects within the upper plate (Hall, 2002; Cawood et al., 2009). Several models have also shown that exhumation and uplift are sensitive to both plate convergence obliquity and the thickness of the subducted oceanic plate (Cloos, 1993; Thompson et al., 1997; Spotila et al., 1998; Spikings et al., 2001, 2008; Cruz et al., 2007; Espurt et al., 2008; Wipf et al., 2008; Gerya et al., 2009). Therefore, the record of exhumation explains the short-term tectonic events which, in turn, have allowed to refine tectonic models for convergent margins. This is particularly useful in regions where young tectonic overprinting or limited exposure of the associated contemporaneous rock record is scarce, or where overimposed events have erased evidence of older ones.

Plate tectonic reconstructions for the northwestern South America-Caribbean interactions suggest that the orogenic cycle began with the Late Cretaceous-Paleogene collision of the front of the oceanic Caribbean plate, which migrated from the Pacific towards an inter-American position (Burke, 1988; Pindell, 1993; Pindell et al., 1998, 2005; Spikings et al., 2000, 2001; Hughes and Pilatasig, 2002; Luzieux et al., 2006; Vallejo et al., 2006, 2009; Cardona et al., 2010a; Van der Lelij et al., in press; Weber et al., 2009, 2010). Subsequent post Eocene relative eastern migration of the Caribbean plate, Pacific subduction and collision of Panama with the northern Andean margin, as well as variations in North America–South America convergence relations, were responsible for strain partitioning and a heterogeneous geological response along the southern margin of the Caribbean plate (Muessig, 1984; Avé Lallemant, 1997; Pindell et al., 1998; Müeller et al., 1999; Spikings et al., 2000; Taboada et al., 2000; Trenkamp et al., 2002; Cortés et al., 2005; Montes et al., 2005, 2010; Pindell and Kennan, 2009). The formation of several isolated massifs surrounded by sedimentary basins in northeastern Colombia is tied to this complex tectonic scenario (Kellogg, 1984; Pindell et al., 1998; Montes et al., 2005, 2010).

Currently, the timing of uplift and the tectonic configuration that shaped these massifs is still not fully resolved (Kellogg and Bonini, 1982; Kellogg, 1984; Montes et al., 2010). In this contribution, low-temperature zircon and apatite (U-Th)/He thermochronology and geobarometric constraints from the Eocene plutonic rocks of the Sierra Nevada de Santa Marta and Serranía de Jarara uplifted massifs, in the Caribbean region of northern Colombia (Fig. 1), were integrated with published geological constraints to characterize the timing and rates of short and long term exhumation. We use these results to reconstruct the time-temperature and time-pressure paths followed by the plutonic rocks in order to understand the tectonothermal evolution of the massifs (Ring et al., 1999). Additional constraints on exhumation from the less topographically expressed Serranía de Jarara are determined with zircon and apatite U-Th/He thermochronology from Eocene granitoid clasts found in a Late Oligocene conglomerate sampled at the foothills of the Serranía de Jarara (Lockwood, 1966; Zapata et al., in press). We relate the record of Cenozoic exhumation of the two massifs to the evolution of the Caribbean–South American plate tectonic interactions and analyze the results in terms of changes in the paleogeography of the region.

TECTONIC SETTING

The Cenozoic orogenic make-up of the Northern Andes and the Caribbean is related to the interactions of multiple plate boundaries (Caribbean, Pacific and South American plates) and the collision of several oceanic terranes with

the South American margin (Pindell et al., 1998, 2005; Kellogg and Vega, 1995; Hughes and Pilatasig, 2002; Kerr et al., 2003; Vallejo et al., 2006, 2009; Jaillard et al., 2008, 2010; Pindell and Kennan, 2009). Advances in regional plate tectonic modeling have suggested that the Pacific-derived Caribbean oceanic plate drifted towards the East (relative to the Americas) during the Late Cretaceous-Cenozoic and that it obliquely collided with the continental margin during the Late Cretaceous and Paleogene (Pindell et al., 1998, 2005; Spikings et al., 2000, 2001; Kerr et al., 2003; Gómez et al., 2005; Montes et al., 2005; Vallejo et al., 2006, 2009; Cardona et al., 2010a). Continued relative eastern migration of the Caribbean plate built an array of strike-slip dominated orogenic blocks and basins linked to a composite transpressional and transtensional configuration (Muessig, 1984; Macellari, 1995; Pindell et al., 1998, 2005; Pérez de Armas, 2005; Beardsley and Avé Lallemant, 2007; Cruz et al., 2007; Montes et al., 2010).

Additional Cenozoic tectonic factors that have influenced this segment of the South American margin include: 1) changes in convergence direction and rate between North and South America and associated relative displacements of the Caribbean plate (Pindell et al., 1988; Müeller et al., 1999; Pindell and Kennan, 2009); 2) forced subduction of a thick Caribbean oceanic plate (Mauffret and Leroy, 1997; Pindell et al., 2005); 3) Early Eocene changes in convergence direction between the Pacific plates and the South American margin from N-S to WNW-ESE (Pilger, 1984; Pardo-Casas and Molnar, 1987); and 4) the collision of the trailing edge of the Caribbean oceanic plate (Panamá isthmus) with northwestern Colombia (Kellogg and Vega, 1995; Taboada et al., 2000).

The Caribbean–South America plate boundary was also marked by the formation of a Cenozoic sedimentary wedge (South Caribbean deformed belt), together with several

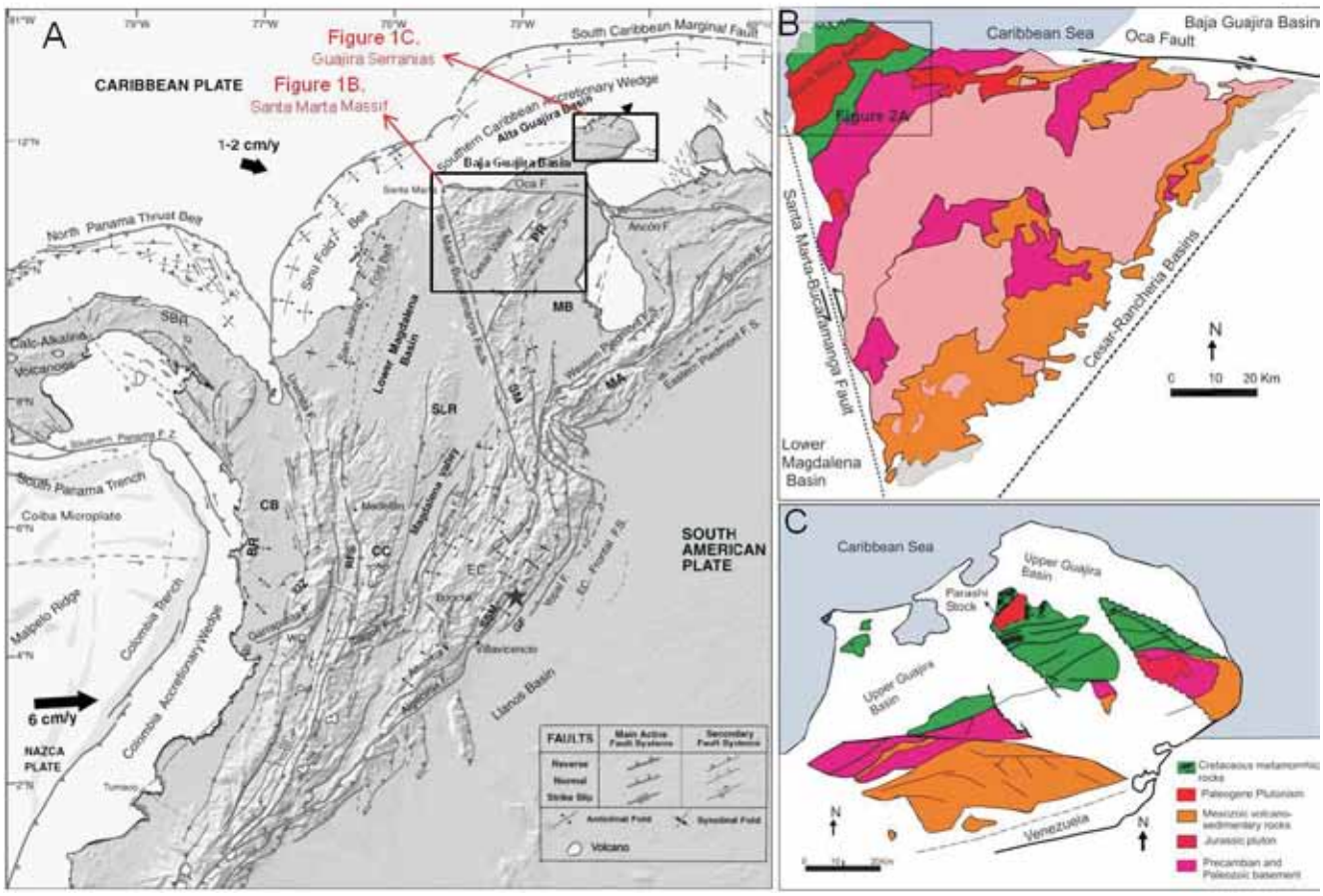

FIGURE 1 | **A) Neotectonic and digital elevation map of the Northern Andes indicating the main active fault systems (after Taboada et al., 2000; Dimate et al., 2003). The Sierra Nevada de Santa Marta, Guajira Serranías and surrounding basins are highlighted on the map. BR: Baudo Range, CB: Chocó Block, CC: Central Cordillera, EC: Eastern Cordillera, GF: Guaicaramo Fault, MA: Mérida Andes, MB: Maracaibo Block, PR: Perija Range, RFS: Romeral Fault System, SLR: San Lucas, SM: Santander Massif, SSM: Servitá–Santa María Fault, WC: Western Cordillera, SBR: San Blas Range, IDZ: Istmina deformation zone. B) and C) Geological sketch maps of the Sierra Nevada de Santa Marta massif and the Guajira region including Serranía de Jarara, respectively.**

pull-apart style basins, uplifted massifs and fold-and-thrust belts (Case et al., 1984; Duque-Caro, 1984; Kellogg, 1984; Muessig, 1984; Lugo and Mann, 1995; Avé Lallemant, 1997; Taboada et al., 2000; Gorney et al., 2007). Within this scenario the Northern Andean margin was segmented into several blocks or microplates that were displaced to the North and East towards the Caribbean realm (Kellogg, 1984; Kellogg and Vega, 1995; Montes et al., 2010).

Recent GPS measurements and stress analyses have shown an oblique East-Southeast convergence of 20±2mm/a between the Caribbean and South American plates demonstrating the North Andean block is still escaping to the northeast (Perez et al., 2001; Weber et al., 2001; Trenkamp et al., 2002; Colmenares and Zoback, 2003). Although most of the convergence is accommodated by major strike-slip zones and earthquake distribution, microseismicity studies and seismic tomographic models have suggested the existence of a slab dipping under the northern segment of the South American margin and the underthrusting of the Caribbean plate against South America (Kellogg and Bonini, 1982; Toto and Kellogg, 1992; van der Hilst and Mann, 1994; Malavé and Suarez, 1995; Miller et al., 2009).

SANTA MARTA AND GUAJIRA

In northern Colombia, the physiographic continuity of the Andean Cordillera changes to a series of isolated uplifted crystalline massifs limited by major strike-slip systems (Fig. 1), and surrounded by barely exposed Cenozoic basins filled with as much as ca. 6km of sediments (Fig. 1, reviews in Guzmán, 2007; Cerón et al., 2007; Rincón et al., 2007). Palinspastic restorations based on basement correlations and structural compatibility have suggested that these massifs were part of a continuous Andean Cordillera during the Late Cretaceous to Early Paleogene, and were later fragmented by Cenozoic Caribbean tectonics (Duque-Caro, 1979; Montes et al., 2005, 2010).

These major uplifted crystalline massifs include the Santa Marta massif and the Guajira Serranías (Simarua, Jarara and Macuira) with elevations as high as ca. 5777m and ca. 600m respectively (Fig. 1). They are both part of the Maracaibo microplate (Burke et al, 1984), which also includes other uplifted regions such as the Serranía de Perijá and the Mérida Andes of Colombia and Venezuela. It is remarkable that the ca. 5777m topography of the Santa Marta massif is characterized by a major positive gravity anomaly and an apparent high geothermal gradient, suggesting a lack of isostatic equilibrium related to recent uplift (Case and MacDonald., 1973; Cerón-Abril, 2008).

Both massifs can be divided into three roughly correlative lithological belts with a well-defined southeast-northwest younging pattern (Fig. 1B and 1C). The older southeastern segment includes ca. 1.2-1.0Ga inliers of high-grade metamorphic rocks (reviews in Tschanz et al., 1974; Cordani et al., 2005; Cardona et al., 2010b) which are intruded/covered by Jurassic to Early Cretaceous plutonic/volcanic rocks (Tschanz et al., 1974; MacDonald and Opdyke, 1972; Cardona-Molina et al., 2006). The intermediate belt is made up of amphibolites and mica schists of Paleozoic age and Permo-Carboniferous mylonitic granitoids (Tschanz et al., 1969, 1974; Cardona-Molina et al., 2006; Cardona et al., 2010c; Weber et al., 2009). The youngest belt includes an imbricate series of Cretaceous greenschist to amphibolite facies metavolcano-sedimentary units and orthogneisses in Santa Marta (Doolan, 1971; MacDonald et al., 1971; Tschanz et al., 1974; Cardona et al., 2010b), and greenschist metasediments with intercalated serpentinites and gabbros in Guajira (Lockwood; 1966; Weber et al., 2010). The three different lithostratigraphic belts are intruded by Eocene I-type plutonic bodies (Tschanz et al., 1974; Mejía et al., 2008; Cardona et al., 2008; Duque et al., 2009), such as the Santa Marta batholith, comprised of quartzdiorites, granodiorites and tonalites. In the Guajira Peninsula, Paleogene plutonism is restricted to the Eocene Parashi stock, a quartzdiorite body with associated porphyritic dikes (Lockwood, 1966; Cardona et al., 2007).

Two Cenozoic basins limit the studied massifs (Fig. 1): 1) the Late Cretaceous to Paleogene Cesar-Ranchería basin, exposed in the southeastern flank of the Santa Marta massif (Bayona et al., 2007; Ayala-Calvo et al., 2010) and 2) the Lower Magdalena and the Baja and Alta Guajira basins, limited by major strike-slip faults and characterized by an extensive post-Oligocene record (Duque-Caro, 1979; Guzmán, 2007; Rincón et al., 2007; Vence, 2008).

ANALYTICAL METHODS

U/Pb LA-MC-ICP-MS geochronology

U/Pb analyses for one granitoid clast were done at the Arizona LASERCHRON laboratory following the procedures described by Gehrels et al. (2008). Results are included in Table 1.

Zircon crystals were analyzed in polished epoxy grain mounts with a Micromass Isoprobe Multicollector Inductively Coupled Plasma-Mass Spectrometry (ICP-MS) equipped with nine Faraday collectors, an axial Daly collector, and four ion-counting channels. The Isoprobe is equipped with an ArF Excimer laser ablation system, which has an emission wavelength of 193nm. The collector

configuration allows measurement of ^{204}Pb in the ion-counting channel while ^{206}Pb, ^{207}Pb, ^{208}Pb, ^{232}Th and ^{238}U were simultaneously measured with Faraday detectors. All analyses were conducted in static mode with a laser beam diameter of 35-50μm, operated with an output energy of ~32mJ (at 23kV) and a pulse rate of 9Hz. Each analysis consisted of one 20-second integration on peaks with no laser firing and 20 one-second integrations on peaks with laser firing. Hg contribution to the ^{204}Pb mass position was removed by subtracting on-peak background values. Inter-element fractionation was monitored by analyzing an in-house zircon standard, which has a concordant Thermal Ionization Mass Spectrometry (TIMS) age of 564±4Ma (2σ). This standard was analyzed once for every five unknowns. Uranium and Th concentrations were monitored by analyzing a standard (NIST 610 Glass) with ~500ppm Th and U. The lead isotopic ratios were corrected for common Pb, using the measured ^{204}Pb, assuming an initial Pb composition according to Stacey and Kramers (1975) and respective uncertainties of 1.0, 0.3 and 2.0 for $^{206}Pb/^{204}Pb$, $^{207}Pb/^{204}Pb$ and $^{208}Pb/^{204}Pb$.

The age of the standard, calibration correction of the standard, composition of common Pb, and the decay constant uncertainty are grouped and known as the systematic error. For these samples the systematic error is of 2.1% for $^{206}Pb/^{238}U$ and $^{206}Pb/^{207}Pb$. Uranium-lead age was calculated using Isoplot (Ludwig, 2003). The final crystallization ages that we report were calculated using the TUFFZIRC algorithm. This algorithm was elaborated by Ludwig and Mundil (2003) to minimize the effect of minor inheritance or subtle Pb loss. The reported ages are one sigma level and report only analytical error. The final age error was calculated using two uncertainties: the first is derived from the uncertainty of the TUFFZIRC age calculation alone, the second represents the systematic uncertainty during that session (~1.1%). The age uncertainty is determined as the quadratic sum of the TUFFZIRC error plus the total systematic error for the set of analyses (~1.2%).

Mineral Chemistry

We analyzed the mineral chemistry of amphiboles from eight granitoid samples using a CAMECA SX-50 electron microprobe at the Department of Lunar and Planetary Sciences at the University of Arizona. Analyses were performed with a beam current of 20.0nA and an accelerating voltage of 15kV. Counting time was 10s for sodium and 20s for the rest of the elements.

TABLE 1 | **U-Pb LA-MC-ICP-MS zircon results from the granitoid conglomerate clast of the Oligocene Siamana Formation, Guajira Peninsula**

				Isotope ratios									Apparent ages (Ma)					
Analysis	U (ppm)	206Pb 204Pb	U/Th	206Pb* 207Pb*	± (%)	207Pb* 235U*	± (%)	206Pb* 238U	± (%)	error corr.	206Pb* 238U*	± (Ma)	207Pb* 235U	± (Ma)	206Pb* 207Pb*	± (Ma)	Best age (Ma)	± (Ma)
MSZH4-1	392	5058	4.7	24.1300	13.2	0.0455	13.3	0.0080	2.1	0.16	51.1	1.1	45.1	5.9	-260.3	334.7	51.1	1.1
MSZH4-2	357	7228	5.0	10.9333	2.0	0.3847	5.0	0.0305	4.5	0.91	193.7	8.6	330.5	14.0	1456.3	38.8	193.7	8.6
MSZH4-3	291	2688	8.6	21.2063	13.9	0.0487	14.5	0.0075	3.9	0.27	48.1	1.9	48.3	6.8	57.1	333.9	48.1	1.9
MSZH4-10	438	19359	1.9	16.7475	5.0	0.1478	8.1	0.0180	6.4	0.79	114.7	7.3	140.0	10.6	593.1	107.7	114.7	7.3
MSZH4-11	344	4715	3.5	21.9573	11.9	0.0496	12.1	0.0079	1.9	0.16	50.7	0.9	49.1	5.8	-26.5	289.4	50.7	0.9
MSZH4-13	521	53792	3.9	13.0216	5.1	1.0122	5.5	0.0956	2.3	0.41	588.6	12.8	710.0	28.3	1115.9	100.9	588.6	12.8
MSZH4-14	269	3595	7.9	19.5746	15.2	0.0555	15.4	0.0079	2.7	0.18	50.6	1.4	54.8	8.2	244.7	351.7	50.6	1.4
MSZH4-15	314	2842	4.0	21.0630	17.6	0.0494	17.7	0.0075	1.5	0.09	48.4	0.7	48.9	8.4	73.2	421.4	48.4	0.7
MSZH4-16	267	4683	4.3	16.6159	6.4	0.1074	11.9	0.0129	10.0	0.84	82.9	8.2	103.6	11.7	610.2	138.4	82.9	8.2
MSZH4-17	256	2006	3.3	21.0117	13.9	0.0499	14.0	0.0076	2.0	0.14	48.8	1.0	49.4	6.8	79.0	330.8	48.8	1.0
MSZH4-18	512	58450	11.6	14.6247	3.2	0.5186	7.9	0.0550	7.2	0.91	345.2	24.2	424.2	27.4	880.0	66.8	345.2	24.2
MSZH4-19	310	3241	6.3	24.5172	28.6	0.0434	##	0.0077	1.5	0.05	49.5	0.7	43.1	12.1	-300.8	743.4	49.5	0.7
MSZH4-20	378	669	2.5	25.3224	17.6	0.0407	17.8	0.0075	2.3	0.13	48.0	1.1	40.5	7.1	-384.1	461.0	48.0	1.1
MSZH4-21	341	599	4.1	19.5481	24.5	0.0519	##	0.0074	3.0	0.12	47.2	1.4	51.4	12.4	247.9	571.9	47.2	1.4
MSZH4-22	557	75226	2.2	15.3075	2.8	0.7416	7.6	0.0823	7.1	0.93	510.1	34.6	563.4	32.9	784.9	59.0	510.1	34.6
MSZH4-23	335	4176	7.4	23.7333	11.1	0.0460	11.1	0.0079	0.5	0.05	50.8	0.3	45.6	5.0	-218.4	279.6	50.8	0.3
MSZH4-25	553	20412	2.9	18.3900	1.5	0.3185	3.5	0.0425	3.2	0.91	268.2	8.4	280.7	8.7	386.7	33.7	268.2	8.4
MSZH4-26	233	511	2.2	16.7391	9.6	0.0612	9.7	0.0074	1.4	0.14	47.7	0.6	60.3	5.7	594.2	208.3	47.7	0.6
MSZH4-28	434	3161	2.1	19.6400	11.0	0.0524	11.1	0.0075	1.8	0.16	47.9	0.8	51.9	5.6	237.0	253.9	47.9	0.8
MSZH4-29	238	3826	8.5	23.1339	17.3	0.0490	17.4	0.0082	2.0	0.11	52.8	1.0	48.6	8.3	-154.5	432.5	52.8	1.0
MSZH4-30	560	6664	2.9	22.1199	5.1	0.0480	6.1	0.0077	3.4	0.56	49.5	1.7	47.6	2.9	-44.4	124.0	49.5	1.7

Microprobe analytical error varies roughly between ±0.01 and 0.04wt% (1 sigma [1σ]). Analytical results are presented in Table I (electronic appendix available in www.geologica-acta.com).

(U-Th)/He thermochronometry

Apatite and zircon concentrates were obtained through the conventional method of heavy liquid-magnetic susceptibility separation. From a non-magnetic mineral fraction, apatite and zircon crystals were hand-picked using a high-power (180x) stereozoom petrographic microscope with cross-polarization which allows inclusion screening under reflected and transmitted light. When possible, mostly transparent, inclusion-free, euhedral, unfractured grains with similar shape and size were selected (average prism width ~80±10μm, length/width ratios of less than 1.5). Uniform grain size minimizes differences in He diffusion behavior (Farley, 2000; Hourigan et al., 2005). Sizes >60-70μm require low correction factors for He ages and increases accuracy (Farley, 2002). Selected grains were digitally photographed and geometrically characterized by measuring each grain for its prism length (parallel to the c axis) and prism width in at least two different orientations (perpendicular to the c axis). Measurements were used to perform alpha ejection corrections (Ft) (Farley, 2002).

All (U-Th)/He analytical procedures were performed at the University of Arizona Radiogenic Helium Laboratory following a protocol based on methods reported for apatite (House et al., 1999, 2000; Stockli et al., 2000; Farley, 2002) and for zircon (Reiners, 2005; Farley, 2002). Helium isotopic measurements were made by degassing each sample replicate through laser heating and evaluating ^{4}He by isotope-dilution gas source mass spectrometry. Radiogenic He was analyzed using a fully-automated mass spectrometry system consisting of a Nd-YAG laser for total He laser extraction, an all-metal, ultra-high-vacuum extraction line, a precise volume aliquot system for ^{4}He standard and ^{3}He tracer for isotopes, a cryogenic gas purification system, and a Blazers Prisma QMS-200 quadrupole mass spectrometer for measuring $^{3}He/^{4}He$ ratios. Two single-grain aliquots per sample were prepared following the standard protocol available at the University of Arizona. Determination of U, Th, and Sm were performed on the same crystals by isotope-dilution ICP-MS on a Thermo Element 2 ICP-MS also at the University of Arizona. Mean (U-Th)/He ages were calculated on the basis of two apatite and zircon replicate analyses.

Zircon He dating

Measurements of parent and daughter nuclides in zircon grains were performed on two single-grain aliquots per sample following the protocol presented in Reiners (2005). To minimize potential zonation effects, grains without obvious inclusions were chosen. Clear, non-magnetic, tetragonal crystals with prism widths of at least 75-100μm were preferred while grains with prism widths <60μm were avoided. Morphologies most similar to a tetragonal prism with bipyramidal terminations were selected because alpha-ejection corrections entail the assumption of this characteristic grain morphology (Reiners, 2005; Hourigan et al., 2005). Irregular morphologies, elongated grains or crystals with fractured surfaces at low angles relative to the *c*-axis were rejected. Selected crystals were photographed and their dimensions measured in two perpendicular perspectives parallel to the *a*1 and *a*2 crystallographic axes. Measured dimensions and an assigned morphology were used to calculate the alpha-ejection correction following the Ft correction scheme of Farley (2002). The extraction involved placement of a single crystal into a ~1mm Nb foil packet that was then slightly closed and placed on a Cu planchet with another few dozen sample slots in a high-vacuum sample chamber connected to the He purification/measurement line. Each foil packet was directly heated using a 10μm focused laser beam of a 1064-nm Nd-YAG laser to ~1100–1250°C for 15 minute extraction intervals. All samples were then subjected to at least two re-extractions and He measurements, to assess the extent of degassing of the crystal (typical re-extracts yielded less than 0.5% of previous ^{4}He values). Helium extracted from zircons was spiked with ~0.1-1.0pmol ^{3}He, cryogenically concentrated and purified, and expanded into a small volume with a gas-source quadrupole mass spectrometer. Ratios of $^{4}He/^{3}He$ were measured for about ten seconds following gas release and nominal equilibration time. Measured ratios were corrected for background and interferences on mass 3 (HD+ and H3+), and compared with $^{4}He/^{3}He$ measured on pipetted aliquots of a manometrically calibrated ^{4}He standard processed by the same methods. ^{4}He in the unknown zircon is assumed to be the product of the ^{4}He content of the standard with $^{4}He/^{3}He$ ratio measurements on the unknown and the standard.

Uranium and thorium nuclides in degassed zircons were measured by isotope dilution and solution ICP-MS. The approach required spiking with isotopically distinctive U-Th spike, sample-spike equilibration, and dissolution to a final solution suitable for ICP-MS. Zircon dissolution was carried out using $HF\text{-}HNO_3$ mixtures which can dissolve the entire Nb foil and zircon content in Parr bombs at temperatures and pressures higher than ambient. Ratios of $^{238}U/^{233}U$ and $^{232}Th/^{229}Th$ were quantified by 2000 measurements of the average intensities in the middle 10% of peak widths in low resolution mode on an Element2 high-resolution ICP-MS. $^{238}U/^{235}U$ was also measured to check for Pt contamination and mass fractionation. The zircon content in U and Th was calculated from multiple determinations of isotope ratios

on pure spike and spiked normals containing 1–4ng of isotopically normal U and Th.

In zircon, He dating alpha ejection was corrected using the method of Farley et al (1996) and Farley (2002). The analyzed standard included zircons from the Fish Canyon Tuff with two standard analyses per sample batch. This standard has been routinely calibrated, yielding a (U-Th)/He age of 28.29±0.26Ma in one hundred and fourteen grains (95%; 2s external error of 2.6Ma or 9.3%, MSWD=20). Fish Canyon zircon analyses carried out during this work are included within Tables 2 and 3.

Propagated errors for zircon He ages based on the analytical uncertainty associated with U, Th, and He measurements are ~4% (2σ) for laser samples (Reiners, 2005; Farley, 2002). Nevertheless, a 6% (2σ) uncertainty for all samples is reported based on the reproducibility of replicate analyses of laboratory standard samples (Reiners, 2005). All analytical results are presented in Table 2.

Apatite He dating

Single-grain aliquots were prepared and two replicate analyses were performed for each sample. After careful optical screening, apatite crystals were placed into 0.8mm Nb packets, which were then loaded into stainless steel sample planchets. Each sample replicate was degassed via laser heating for 3 minutes utilizing a Nd-YAG laser at 1.5W to attain temperatures of ~1050°C and then analyzed for ^{4}He, followed by a second extraction (He re-extraction) to ensure complete degassing and to monitor He release from more retentive U- and Th-bearing inclusions in analyzed apatite. Helium blanks (0.05.0.1fmol ^{4}He) were determined by heating empty Nb foil packets using the same procedure. Gas extracted from samples was processed by: 1) spiking with ~4pmol of ^{3}He; 2) concentrating in a cryogenic system at 16ºK on a charcoal trap, and purification by release at 37ºK; and 3) measuring ^{4}He/^{3}He ratios (corrected for HD and H3 by monitoring H+) on a quadrupole mass spectrometer. All ratios were referenced to multiple same-day measured ratios and known volumes of ^{4}He standards processed in a similar fashion.

Once ^{4}He measurements were completed, samples were retrieved from the laser cell, placed in Teflon® vials, dissolved in ~30% HNO_3, and spiked with mixed ^{230}Th-^{235}U-^{149}Sm tracer for isotope dilution ICP-MS analysis of U, Th, and Sm. Each batch of samples was prepared with a series of acid blanks and spiked normals to monitor the purity and calibration of reagents and spikes. Spiked samples were analyzed as 0.5mL of ~1.5ppb U-Th solutions by isotope dilution on a Thermo Element 2 ICP-MS. Precision and sensitivity of the instrument allow isotopic analyses with RSD <1%. Concentrations of ^{147}Sm were close to zero for all samples. Th/U rations were used to monitor for the presence of Th rich phases such as monazite. The mean Th/U for all of the replicates combined is 0.9 and most values are below 1 so none of the analyses had to be excluded.

Alpha ejection was corrected for apatite He ages using the method of Farley et al., 1996, Farley, 2002). Durango apatite standards were run during each batch of unknown samples (every 9 unknowns) to monitor system performance and check analytical accuracy. Durango is a well-characterized apatite from Durango, México with a reference Ar-Ar age of 31.44±0.18Ma (2σ) and a (U–Th)/He age of 31.13±1.01Ma (±1 S.E.=0.21) (McDowell et al., 2005). Replicate aliquots of this standard yield an average age of 31.9Ma, with two standard deviations of 2.2Ma (6.6%), and a weighted mean age and error of 31.94±0.17Ma (95% confidence interval, with a 2s required external error of 1.9Ma or 5.9%, MSWD=5.4).

Analytical uncertainties for the University of Arizona (U-Th)/He facility are assessed ~6% (2σ), which incorporate noble gas analysis and ICP-MS uncertainties. Propagated errors for apatite He ages based on the analytical uncertainty associated with U, Th, and He measurements are 4% (2σ) for laser samples. A 6% (2σ) uncertainty for all samples is reported based on the reproducibility of replicate analysis of laboratory standard samples (Reiners, 2005). All analytical results are presented in Table 3.

SAMPLING

In order to constrain the Cenozoic exhumation history we focused on the thermochronology of the northwestern segment of the Santa Marta and the Serranía de Jarara uplifted massifs, where the younger record consists mainly of Eocene plutonic rocks (Lockwood, 1966; Tschanz et al., 1969). In the Santa Marta massif, quartzdiorite and granodiorite samples of the Eocene Santa Marta batholith and a host orthogneiss were taken along an elevation profile near the coastal region (Fig. 2A, 2B). Elevations from the sampled transect range 189m to 1609m within a horizontal distance of ca. 26km. Recent U/Pb geochronology from the Santa Marta batholith has shown an evolution with two contrasting phases of magmatism during 65-62Ma and 58-50Ma (Cardona et al., 2008; Duque et al., 2009). Recovered samples are from the youngest pulse, together with an additional orthogneiss sample that has a crystallization age of ca. 92Ma (Cardona et al., 2008). In contrast, relief in the Guajira Serranías is lower, and Paleogene plutonism is restricted to the Parashi stock, which is exposed at only ca. 100m elevation in the northwestern Serranía de Jarara (Lockwood, 1966, Fig. 2B). Unpublished

TABLE 2 | **U-Th/He zircon results from the Santa Marta batholith and Parashi stock**

	mass (ug)	U ppm	Th ppm	4He (nmol/g)	HAC	Age (Ma)	1s err (Ma)	Elevation (m)	North	E or W
Santa Marta Batholith										
EAM-18-72A	8.93	178.70	87.98	18.28	0.79	21.45	0.68	130	1713860	989845
EAM-18-72B	7.91	158.06	71.01	16.17	0.78	21.97	0.50	130	1713860	989845
EAM-11-43A	2.09	542.19	297.41	55.34	0.69	24.14	0.56	189	1728142	992387
EAM-11-43B	1.16	162.72	44.40	11.09	0.63	18.74	0.59	189	1728142	992387
EAM-11-42A	3.47	209.59	97.19	21.49	0.74	23.18	0.55	252	1726304	993827
JRG-11-15A	8.98	355.34	82.46	35.41	0.80	21.96	0.46	617	1723670	995183
JRG-11-15B	5.05	253.46	65.55	26.20	0.77	23.38	0.49	617	1723670	995183
EAM-11-50A	2.37	403.50	118.57	35.47	0.71	21.56	0.59	943	1722398	997166
EAM-11-50B	6.13	426.32	144.28	51.53	0.77	26.82	0.55	943	1722398	997166
EAM-19-66A	9.46	184.25	36.61	17.23	0.80	20.64	0.56	1430	1719467	999600
EAM-19-60A	5.30	969.79	114.18	98.68	0.74	24.73	0.67	1569	1715731	1003817
EAM-19-60B	4.05	933.69	69.91	77.67	0.75	20.33	0.37	1569	1715731	1003817
EAM-19-59A	6.02	509.65	582.56	70.10	0.77	26.19	0.49	1602	1717331	1003526
EAM-19-59B	19.94	307.86	358.18	40.20	0.84	22.50	0.42	1602	1717331	1003526
Parashi Stock										
CM-3-2A	5.21	167.33	64.50	27.56	0.77	36.51	0.73	150	12º 13' 46"	71º 41' 20.9"
CM-3-2B	3.29	207.62	77.09	34.16	0.73	38.36	0.74	150	13º 13' 46"	72º 41' 20.9"
CM-3-7A	13.21	111.46	59.98	18.88	0.83	33.40	0.68	165	12º 13' 05.2"	71º 40' 48.1"
CM-3-7B	15.24	302.02	159.63	54.46	0.83	35.58	0.63	165	13º 13' 05.2"	72º 40' 48.1"
CM-5-20A	12.48	136.25	59.70	24.53	0.82	36.77	0.74	170	12º 13' 34.8"	71º 44' 36.7"
CM-5-20B	17.40	101.76	48.84	19.44	0.84	37.79	0.72	170	13º 13' 34.8"	72º 44' 36.7"
Oligocene conglomerate										
MSZH-04A	3.90	345.74	75.28	69.28	0.74	47.36	0.98	120	12°17´13"	71°41´31"
MSZH-04B	2.92	440.96	65.63	85.95	0.72	48.69	0.96	120	12°17´13"	71°41´31"
MSZH-06A	0.71	372.43	89.28	51.60	0.55	44.58	0.94	120	12°17´18.3"	71°41´31"
MSZH-06B	1.96	570.59	155.92	105.61	0.68	47.25	0.96	120	12°17´18.3"	71°41´31"

TABLE 3 | **U-Th/He apatite results from the Santa Marta batholith and Parashi stock**

	mass (ug)	U ppm	Th ppm	Sm ppm	4He (nmol/g)	HAC	Age	1s err (Ma)	Elevation (m)	North	E or W	Weight average	MSWD
Santa Marta Batholith													
EAM-18-72A	8.75	160.36	327.63	122.69	9.36	0.79	9.21	0.19	130.00	1713860	989845	9.72	0.31
EAM-18-72B	4.12	90.48	140.83	88.67	5.47	0.75	10.89	0.28	130.00	1713860	989845		
EAM-11-43A	2.13	42.14	33.26	72.64	1.60	0.69	8.66	0.49	189.00	1728142	992387	7.6	0.8
EAM-11-43B	1.24	27.40	16.53	53.73	0.62	0.67	5.51	0.69	189.00	1728142	992387		
EAM-11-42A	0.93	18.04	23.66	147.42	0.49	0.62	6.22	1.28	252.00	1726304	993827	8.9	1.6
EAM-11-42B	1.60	14.72	29.01	136.06	0.83	0.66	10.77	1.05	252.00	1726304	993827		
JRG-11-15A	1.78	77.95	12.27	93.90	3.40	0.67	11.70	0.48	617.00	1723670	995183	14.68	5.9
JRG-11-15B	4.50	66.52	34.50	86.09	4.94	0.74	16.44	0.37	617.00	1723670	995183		
EAM-11-50A	1.28	11.41	4.15	27.35	0.55	0.64	12.87	2.40	943.00	1722398	997166	13.7	4
EAM-11-50B	1.04	11.67	0.86	49.61	0.62	0.62	15.68	3.65	943.00	1722398	997166		
EAM-19-66A	2.79	12.41	25.00	38.87	0.62	0.72	8.71	0.72	1430.00	1719467	999600	9	1.2
EAM-19-66B	2.34	9.67	1.14	22.00	0.37	0.71	9.76	1.15	1430.00	1719467	999600		
EAM-19-60A	1.08	8.68	5.11	47.55	0.45	0.63	13.26	2.96	1569.00	1715731	1003817	14.4	0.21
EAM-19-60B	0.84	19.34	5.11	121.68	1.04	0.62	15.03	2.23	1569.00	1715731	1003817		
EAM-19-59B	0.76	10.88	21.17	60.69	1.25	0.59	24.57	3.51	1602.00	1717331	1003526	24.57	7.01
Parashi Stock													
CM-5-20A	5.11	7.74	15.70	96.17	1.51	0.74	32.55	0.61	150	12º 13' 34.8"	71º 44' 36.7"		
CM-3-7A	2.87	6.27	14.27	85.75	1.01	0.72	26.54	0.66	165	12º 13' 05.2"	71º 40' 48.1"		
CM-3-2A	6.50	6.48	11.82	127.33	1.20	0.77	30.44	0.51	170	12º 13' 46"	71º 41' 20.9"		
CM-3-2B	8.16	7.32	13.80	158.88	1.41	0.79	30.73	0.61	170	13º 13' 46"	72º 41' 20.9"		
Oligocene conglomerate													
MSZH-04A	3.56	3.96	5.17	123.10	0.83	0.70	40.82	1.03	120	12°17´13"	71°41´31"		
MSZH-04B	4.69	4.13	6.67	121.02	0.93	0.76	38.82	0.80	120	12°17´13"	71°41´31"		
MSZH-06A	7.09	5.74	7.24	95.90	1.14	0.76	36.66	0.72	120	12°17´18.3"	71°41´31"		

zircon U/Pb geochronology from the Parashi stock has yielded ages between 50 and 46Ma. Three quartzdiorite samples of this granitoid (CM-5-20, CM-3-2 and CM-3-7) were selected for He zircon and apatite thermochronology.

Because of the value of conglomerate clasts to constrain older phases of exhumation (Thomson, 1994; Bernet and Spiegel, 2004; Colgan et al., 2008), we extracted complementary thermochronological information about the Serranía de Jarara from clasts recovered from a Late Oligocene–Early Miocene conglomeratic unit (Lockwood, 1966; Zapata et al., in press). Two granitoid clasts (MSZH-4 and MSZH-6) were selected from the marine fan conglomerate in the foothills of the Serranía de Jarara, near the Parashi stock. Clast counting analysis links the provenance to proximal granitoids and metamorphic rocks in the immediately adjacent Serranía de Jarara (Zapata et al., in press).

RESULTS

U-Pb Geochronology

Uranium-Pb geochronology from the Santa Marta and Jarara Paleogene granitoids has been recently constrained in detail (Cardona et al., 2008; Duque et al., 2009). Results from samples along the analyzed transect in Santa Marta show a magmatic crystallization history between 57 and 50Ma (Cardona et al., 2008), whereas for the Parashi granitoid, newly acquired U-Pb crystallization ages are between 50-46Ma. In order to further understand the origin of the sampled granitoid clasts in the conglomerate, we determined U-Pb zircon crystallization ages from one clast, by means of U-Pb LA-ICP-MS methods. This sample (MSZH-4) was subsequently analyzed for zircon and apatite helium thermochronology.

Twenty-one zircon crystals were analyzed from sample MSZH-4 (Table 1). Fifteen crystal tips yielded a mean age of $^{206}Pb/^{238}U$ of 48.8+1.5-1.1Ma (Fig. 3), calculated following Ludwig and Mundil's (2002) algorithm to minimize the effect of inheritance or subtle Pb loss. Analyses that are statistically excluded from the main cluster are shown in gray on Figure 3. We interpreted this age as the granitoid crystallization age. This age is similar to the U-Pb and hornblende K-Ar ages obtained in the Parashi stock (Cardona et al., 2007) as well as detrital zircon ages found within the conglomerate matrix (Zapata et al., in press).

Granitoid emplacement depths

When the emplacement pressures of temporally constrained granitoid rocks are transformed into paleodepths, they can be used as a valuable reference to reconstruct the denudation and exhumation record (Ring et al., 1999). Emplacement depths were estimated by Al

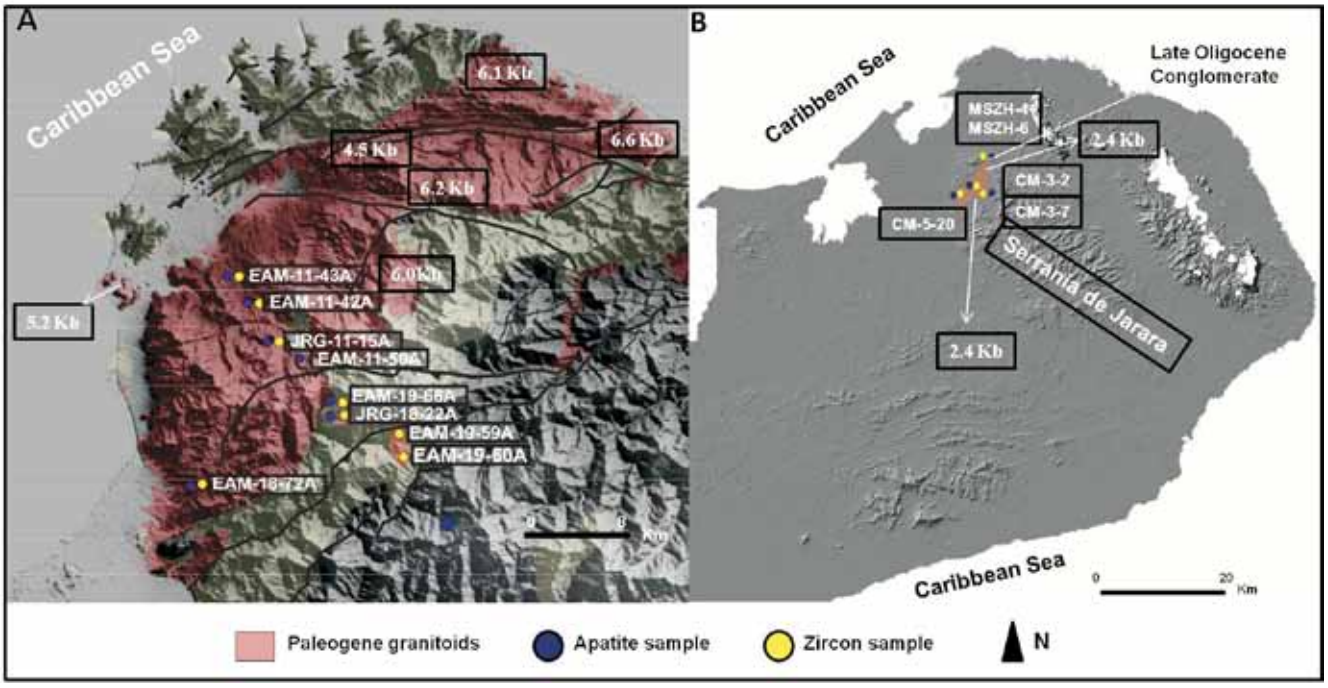

FIGURE 2 | **Digital elevation models and sample locations for A) the Santa Marta and B) Serranía de Jarara regions.**

in-amphibole content of selected granitoid samples from the Santa Marta batholith and the Parashi stock. Analyzed samples from the Santa Marta batholith include amphibole-biotite tonalites and granodiorites. They are composed of plagioclase (43-52%), K-feldspar (2.2-9.2%), quartz (14-29), hornblende (4-21.8%) and biotite (6.2-17%), with titanite, apatite and zircon as accessori. The Parashi stock is made up of granodiorite and quartzdiorite lithotypes. Compositional variations are recorded by amphibole and biotite (12-25%) as well as K-feldspar (7-10.9%). Other minerals show average values of 47.6% (plagioclase) and 22.8% (quartz).

Analytical results of hornblende and pressures calculated using the Schmidt (1992) Al in hornblende calibration are presented in Table I (electronic appendix available in www.geologica-acta.com). All the analyzed amphiboles are calcic and were classified following Leake et al. (1997) in Fig. 4. Pressures obtained from six samples of the Santa Marta batholith vary between 4.9±0.6 and 6.4±0.6kbar. For the Parashi stock, calculated pressures on two samples are lower, between 2.3±0.6 and 3±0.6kbar, and are similar to those reported by Martínez (2008) in other samples from the same stock. These pressure values are consistent with the nature of their host rocks: amphibolite facies rocks with peak pressures of 6.6±0.8kbar in the former (Bustamante et al., 2009; Cardona et al., 2009), and greenschist facies rocks in the latter (Lockwood, 1966). These pressures indicate emplacement depths of 14.7-19.2km and 6.9-9km, respectively.

U-Th/He thermochronology

Santa Marta batholith

Very old ages were discharged due to their lack of coherence and their potential relation with inclusions, which commonly yield older ages (Fitzgerald et al., 2006).

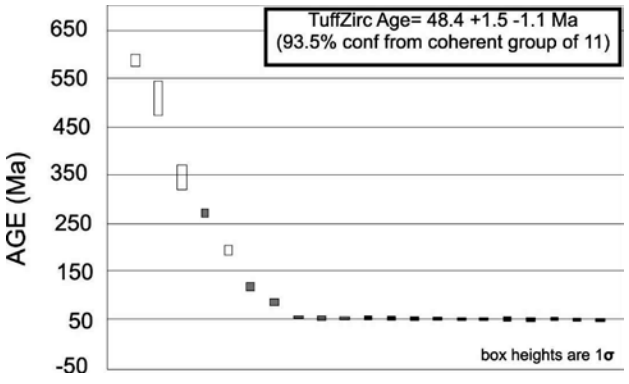

FIGURE 3 | **U-Pb zircon ages from a granitoid clast of the Oligocene conglomerate of Serranía de Jarara, Guajira Peninsula.**

Zircon ages show very poor relation with elevation. The fourteen zircon He ages from nine samples range from 18.7Ma to 26.2Ma (Table 2, Fig. 5). Some of the age variations may be related to local structural disruption. In contrast, apatite He ages extend from 24.6Ma to 5.5Ma (Table 3), showing a well-defined pattern of age increase with elevation (Table 3).

Serranía de Jarara

Elevation of the three samples collected from the Parashi stock varies between 130m and 170m. Zircon U-Th/He ages range from 33.4Ma to 38.4Ma (Table 2), and apatite helium ages are similar, ranging from 30.4Ma to 35.6Ma (Table 3). The two Eocene granitic clasts from the conglomerate yielded older zircon and apatite U-Th/He ages, 48.7-44.6Ma and 40.8-36.7Ma respectively (Tables 2 and 3).

Exhumation rates

He diffusion experiments and age comparisons with other thermochronological systems in slowly cooled rocks have suggested closure temperatures for the U-Th/He system in zircon and apatite in the range of 160-200°C and ca. 70°C respectively (reviews in Farley, 2000; Reiners et al., 2002). For mean upper crust geothermal gradients of 20 and 30°C/km, these closure temperatures give exhumation constraints for crustal levels beween 3 and 9km (Farley, 2000).

Extensive U-Pb geochronology on the magmatic rocks of the Santa Marta massif (Cardona et al., 2008; Duque et al., 2009) has shown that the magmatic episode that formed the sampled rocks in the Santa Marta region took place during the Paleocene-Eocene (ca. 58-50Ma). Similar conclusions can be drawn from the Serranía de Jarara, where the Eocene magmatic event is recorded by the 46-50Ma ages obtained in the Parashi stock (Cardona et al., 2009).

Therefore the cooling rates derived from the low-temperature thermochronometers in the in situ sampled granitoids from Santa Marta are related to unroofing. This is also in agreement with the fact that measured zircon-He and apatite-He ages are younger than pluton crystallization ages. In the case of the Jarara granitoid and clasts from the Oligocene conglomerate, it will be discussed below that their zircon-He ages may reflect fast magmatic cooling rather than unroofing or exhumation ages.

In order to estimate exhumation rates, we followed three different approaches: 1) multiple systems with different closure temperatures in single rock samples, including (U-Th)/He in zircon and apatite; 2) single (U-Th)/He ages, which yield average cooling rates between

the time of apatite He closure and the present; and 3) age-elevation profiles based on the average between the oldest and the youngest He apatite ages of the profile.

Although the effects of heat advection alter exhumation rates were calculated from very low temperature thermochronometers, such as apatite, these effects are probably not significant since the obtained exhumation rates are not high enough to promote heat advection in the upper crust (Brown and Summerfield, 1997; Mancktelow and Grasemann, 1997).

Santa Marta batholith

Actual geothermal gradients from the corner of the Santa Marta massif and surrounding sediments have been estimated by López and Ojeda (2006) from a bottom simulating reflector. Their results have yielded 20°C/km to 40°C/km geothermal gradients (Cerón-Abril, 2008). We have used these two end member values, which include the typical upper crust geothermal gradient of 30°C/km.

Figure 6A shows the pressure (depth)-time path constructed for the Santa Marta batholith, including the inferred emplacement depths for the granitoid, the assumed geothermal gradients and the associated closure-depths of the discussed thermochronological systems.

The emplacement depths of the granitoid suggest ca. 16km unroofing of the Santa Marta region since ca. 57-50Ma (Fig. 6A). Available biotite and amphibole K-Ar ages yielded values of 48.8±1.7 and 44.1±1.6 (Tschanz et al., 1974). Considering the ca. 16km emplacement level of the Santa Marta batholith, recalculated biotite K-Ar ages of ca. 41Ma after Steiger and Jaeger (1977) radioactive decay constants, and an arc gradient of ca. 30°C/km,

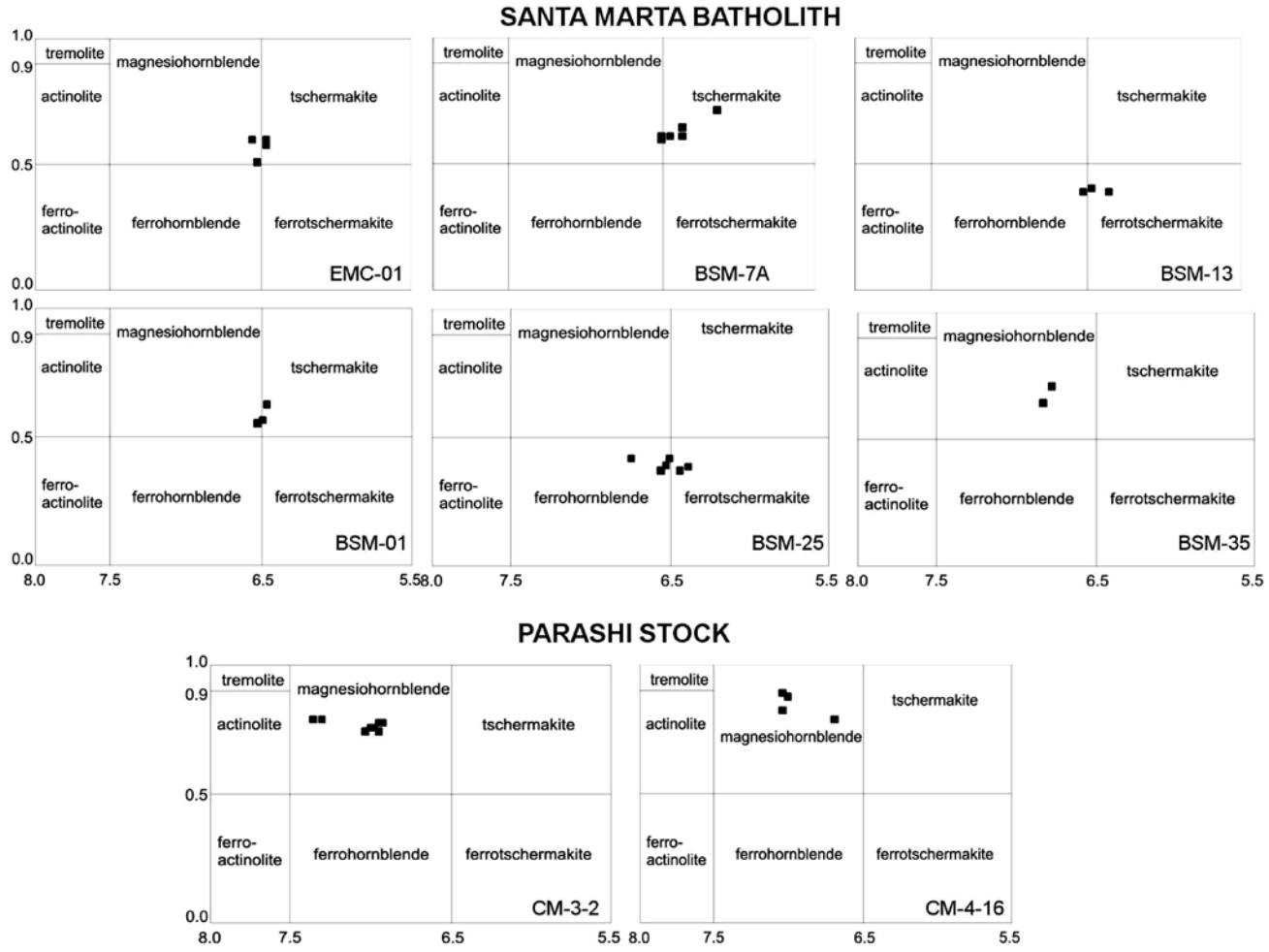

FIGURE 4 | **Composition of amphibole from the analyzed samples of the Santa Marta batholith and the Parashi stock in the amphibole classification scheme of Leake et al. (1997).**

several issues pertaining the higher temperature cooling history and associated exhumation can be reviewed. Comparing an Ar-Ar biotite closure depth of 8.3km (for ca. 250°C closure temperature; McDougall and Harrison, 1999) with the granitoid emplacement depth of ca. 16km, cooling rates between ca. 50-48Ma and 41Ma are of 0.73mm/y. Some of the Santa Marta granitoid exposures showing evidence of an overimposed deformation event in greenschist to amphibolite facies (Tschanz et al., 1969, 1974) probably relate to this exhumation event.

Following this event, between 41Ma and ca. 25Ma, long term exhumation rates seem to diminish down to the range 0.11-0.16mm/y (Fig. 6A), as determined from the biotite cooling depth to zircon-He depths (ca. 6km).

As mentioned, the emplacement depths of the Santa Marta batholith are in the range of 15-19km, which is far from the closure depth of the zircon-He system within the assumed range of geotherms. Therefore, the low temperature zircon- and apatite-He systems can be used to constrain the cooling and exhumation history. The distribution of zircon-He ages with elevation shows a weak variation between 23Ma and 26Ma (Fig. 5) that also reflects fast cooling and associated exhumation at this age. When zircon and apatite closure depths for closure temperatures of 180°C and 70°C are integrated, they vary in the 26-8Ma interval between 0.16 and 0.63mm/y. The lower rates of ca. 0.16mm/y are calculated for samples collected at lower elevation and are considered meaningless. Younger rates (ca. 10-15Ma), determined from the depth of apatite closure temperature and a surface temperature of 10°C, yielded values between 0.09 and 0.48mm/y, with the higher rates determined in samples collected at lower elevations.

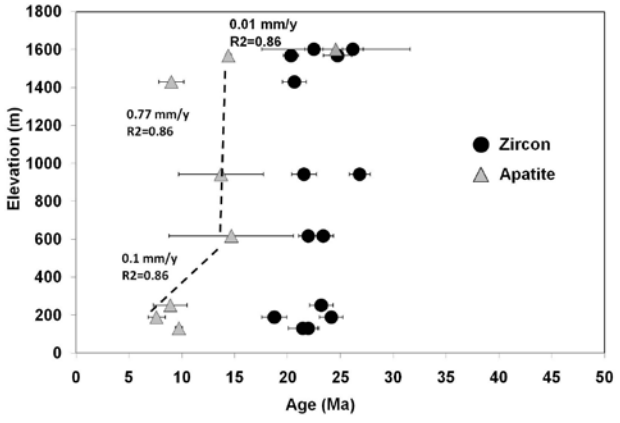

FIGURE 5 | **Santa Marta batholith zircon and apatite U-Th/He elevation profile. Apatite ages are weight average of two analyzed single grain aliquots per sample.**

Weighted average ages for each sample were calculated to construct the elevation profile. The distribution of apatite ages in the elevation profile can be divided into three different segments (Fig. 5). The lower segment, from 189m to 617m with ages between 7 and 14Ma, yields rates of ca. 0.1mm/y. The intermediate segment, from 617m to 1569m, lacks significant age variations (13-14Ma), suggesting the existence of a relatively fast cooling event with rates of 0.77mm/y. The upper segment, although marked by two samples of similar elevation (1569m and 1602m), shows a broader age variation between 14 and 23Ma and suggests very low rates (0.01mm/y).

In order to check for data consistency, we took another granitoid sample in an outcrop located at the southwest of the elevation profile. Sample EAM-18-72, collected at 139m, yielded zircon- and apatite-He ages of ca. 22Ma and 11Ma, respectively, which are similar to those determined for the elevation profile. Cooling rates between 22Ma and 11Ma extracted from this sample also yielded exhumation rates between 0.24 and 0.49mm/y between the depths of closure temperature of zircon and apatite calculated from assumed geothermal gradients of 40°C/km and 20°C/km, respectively. From the apatite data, exhumation rates after 11Ma are 0.13-0.27mm/y (Fig. 5).

In summary, the U-Th/He exhumation analysis for the Santa Marta batholith shows the existence of two relatively fast exhumation events at ca. 24Ma and ca. 15Ma.

Parashi stock

Figure 6B shows the pressure (depth)-time paths constructed for the Parashi stock assuming 20°C/km and 40°C/km geothermal gradients. Crystallization depth for the surface exposure of the Parashi stock ranges between 6.9 and 9km (Fig. 6B). This suggests that at least an equivalent amount of crust has been lost since ca. 48Ma. If stratigraphic relations with discordant Oligocene-Early Miocene conglomerates are considered, this unroofing was already accomplished by ca. 26-23Ma (Fig. 6B).

Biotite K-Ar ages for the Parashi stock granitoid have yielded ca. 45Ma (Lockwood, 1966; Cardona et al., 2007). This age is related to fast magmatic cooling, for it overlaps with hornblende K-Ar ages and are both close in time (less than 5Ma) with the U-Pb zircon crystallization ages. Also, calculated emplacement depths overlaps with zircon-He closure depths, suggesting that the zircon-He ages are related to fast magmatic cooling. On the other hand, similarities between zircon-and apatite-He ages (33.4Ma-38.3Ma and 30.4Ma-35.6Ma) suggest relatively fast cooling related to a Late Eocene exhumation event.

We have reconstructed the exhumation-cooling history of the Parashi stock using the same geothermal gradients (20-40°C/km) and zircon and apatite closure depths (for closure temperatures of 180°C and 70°C, respectively) as above for the Santa Marta region. Exhumation rates between 38Ma and 30.4Ma yielded values between 0.79 and 1.41mm/y. In addition, we considered an upper surface temperature of 10°C to constrain the cooling and exhumation rates after 30.4Ma. Stratigraphic relations with the Oligocene conglomerate suggest that this granitoid was exposed in the Late Oligocene–Early Miocene (ca. 26-23Ma). Therefore, rates between 26 and 23Ma are 0.29-0.98mm/y.

A similar approach was followed for the two conglomerate clasts. Zircon-He ages of 48–44.5Ma in the two clast overlap with the K-Ar biotite and hornblende ages (Lockwood, 1966; Cardona et al., 2007) and suggest that the zircon ages are also related to fast magmatic cooling. Exhumation rates between 48Ma to 36Ma were determined between closure He depths in zircon and apatite. Results vary between 0.51 and 1.46mm/y, which are considered maximum values for these samples, as already discussed, and probably come from the fast cooled and relatively shallow Eocene granitoid.

The younger rates between 36Ma and 23-28Ma yielded 0.13-0.40mm/y, as determined from the closure depth of He in apatite and an estimated Late Oligocene to Early Miocene deposition age for the conglomerate (Lockwood, 1966).

The integrated U-Th/He analyses of the Parashi granitoid suggest the existence of a major phase of exhumation between the Late Eocene to Oligocene (36-24Ma).

TECTONIC IMPLICATIONS

Orogeny in continuously active continental margins is influenced by collisions with arc, plateau or continental terranes, or by the nature of ocean-continent subduction geometry and dynamics (Jarrard, 1986; Silver et al., 1998; Cawood et al., 2009; DeCelles et al., 2009; Ramos, 2009). Whereas the understanding of uplift and deformation mechanisms during collisional events has improved in the last decades, mechanisms related to continuous subduction are less certain. The rate and direction of convergence and the thickness of the subducted oceanic plate have been considered as major factors for uplift and exhumation in subduction systems (Silver et al., 1998; Spikings et al., 2001, 2008; Sobolev and Babeyco, 2005; Oncken et al., 2006; DeCelles et al., 2009; Ramos, 2009; Von Houne and Ranero, 2009).

Increasingly sophisticated plate tectonic and paleogeographic reconstructions of the Circum-Caribbean region have shown that since the Late Cretaceous, the tectonic evolution of northwestern South America including the Northern Andes is linked to the interaction of the allochthonous (Pacific-derived) Caribbean oceanic plate with the South American continental margin (Pindell, 1993; Pindell et al., 1998, 2005; Spikings et al., 2000, 2001; Cortés et al., 2005; Montes et al., 2005; Vallejo et al., 2006, 2009; Jaillard et al., 2010; Kennan and Pindell, 2009; Pindell and Kennan, 2009). Although the positions

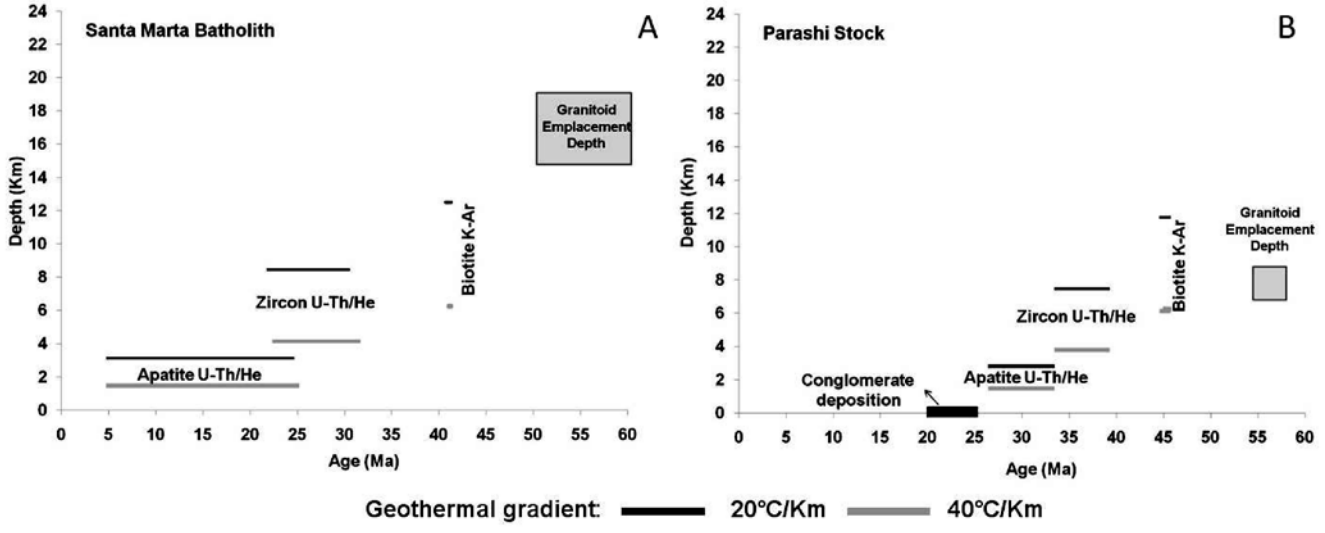

FIGURE 6 | **Depth (pressure)-time paths of A) the Santa Marta Batholith and B) the Parashi stock.**

of the Santa Marta massif and Guajira Serranías have changed throughout the Cenozoic (Muessig, 1984; Macellari, 1995; Bayona et al., 2010; Montes et al., 2010), their paleogeography since the Late Cretaceous is located near the southern margin of the Caribbean plate. Adopting these paleogeographic restrictions, we used the time and rates of exhumation of the Santa Marta batholith and the Parashi stock to test the Cenozoic tectonic scenarios of the Caribbean–South America interactions.

The U/Th-He thermochronological results presented here largely constrain post-Eocene unroofing. Paleogeographic reconstructions suggest that the Caribbean–South American interaction began in the Late Cretaceous when the thick and heterogeneous Caribbean oceanic plate approached the continental margin of South America from an allochthonous Pacific position (Burke, 1988; Pindell, 1993; Mauffet and Leroy, 1997; Pindell et al., 1998, 2005; Pindell and Kennan, 2009). This resulted in an oblique collision of several arc and oceanic plateau lithospheres from Ecuador to the western margin of the Colombian Andes (Pindell, 1993; Kerr et al., 1997; Spikings et al., 2000, 2001; Pindell et al., 2005; Vallejo et al., 2006, 2009; Jaillard et al., 2008). Although this event is not recorded by He thermochronological data, Late Maastrichtian to Paleocene metamorphic remnants that host the sampled granitoids, including high pressure metasedimentary rocks and eclogites in Guajira, are related to this major collisional event (Bustamante et al., 2009; Cardona et al., 2010a; Weber et al., 2007, 2009, 2010). Provenance constraints from Paleocene to Eocene sandstones of the Cesar-Ranchería basins located in the southeastern flank of the Santa Marta massif show major Early Paleocene changes in detrital sources that are related to the uplift of the northwestern segment of the Santa Marta massif (Bayona et al., 2007; Ayala-Calvo et al., 2010).

The Late Cretaceous-Paleogene Caribbean–South American arc-collision orogeny was followed by the eastern displacement of the Caribbean plate in between the margins of the Americas (Müeller et al., 1999; Kennan and Pindell, 2009; Pindell and Kennan, 2009). Plate tectonic reconstructions have shown that, during the Cenozoic, North and South America experienced major changes in the direction and rates of convergence that directly influence the kinematic interaction of the Caribbean and South American plates (Pindell et al., 1988; Müeller, 1999). This includes the transition from a slow and sinistral transtension regime between 83Ma and 55.9Ma that overlaps with the timing of the Late Cretaceous-Paleogene collisional event, to 6.5-1.5mm/y northeast-southwest convergence in the 55.9-38.4Ma interval. Tomographic analyses have also shown the existence of a deep slab below the Maracaibo block that includes the Santa Marta and Guajira regions (van der Hilst and Mann, 1994; Taboada et al., 2000; Miller et al., 2009). Simple plate convergence rate calculations and the current location of the slab as far as the Venezuelan Andes correlate with an inception of this slab in the Maracaibo block since the Early Paleocene, as also suggested by the existence of Late Paleocene to Eocene arc-related plutonism in Santa Marta and Guajira (Cardona et al., 2007, 2008; Duque et al., 2009).

The Santa Marta arc is characterized by a well defined crystallization record between 58-50Ma (Cardona et al., 2008; Duque et al., 2009). Fast magmatic cooling of these granitoids is suggested by a recalculated hornblende K-Ar age of ca. 45Ma from Tschanz et al. (1974) and Ar-Ar ages (Duque et al., 2009). Although fast magmatic cooling is a common feature of intermediate to shallow plutons (Glazner et al., 2004; Parada et al., 2005), the elongated character of this body and the existence of significant mineral orientations at its margins (Tschanz et al., 1969; Duque et al., 2009) suggest that its emplacement was controlled by compressional to transpressional tectonics (Saint Blanquat et al., 1998).

As already mentioned, the published biotite K-Ar ages of ca. 41Ma, in addition to the determined granitoid emplacement depth and the ca. 10Ma between the younger granitoid crystallization ages and the K-Ar cooling age, suggest another relatively fast exhumation event during the Early Eocene (ca. 50-41Ma). Evidences of local overimposed mylonitic deformation in the granitoid rocks including our field observations in the coastal zone may be related to deformation during this exhumation event (Tschanz et al., 1969, 1974).

We therefore suggest that the faster North-South approach between North and South America that ensued the onset of subduction of the Caribbean plate below South America (Pindell et al., 1988; Müeller et al., 1999) facilitated uplift and exhumation in the upper plate during the Middle Eocene (Fig. 7A; Gorczyk et al., 2008). Exhumation was probably accentuated by the effects of the subduction of a thick buoyant Caribbean plate (Cloos, 1993; Mauffret and Leroy, 1997; Spikings et al., 2001, 2008; Espurt et al., 2008; Pindell and Kennan, 2009).

Between 41 and 25Ma, long term exhumation rates on Santa Marta slowed down, contrasting with the 35-30Ma exhumation record in Guajira. Stratigraphical analysis, tectonic reconstructions and paleomagnetism suggest that block rotation in the Santa Marta massif and Guajira region took place during this time interval, forming several transtensional basins in the Guajira region (Fig. 7B, MacDonald and Opdyke, 1972; Muessig, 1984; Macellari, 1995; Vence, 2008; Bayona et al., 2010; Montes et al., 2010). Thus, we suggest that this exhumation phase in Santa Marta and Guajira

is related to the slow transcurrent configuration that characterized the Caribbean-South America interface between 38.4 and 25.8Ma (Müeller et al., 1999; Pindell and Kennan, 2009). The higher Late Eocene rates recorded by the Parashi stock, which extend until the Early Oligocene, may be the result of more severe block rotation and displacements on the Guajira Peninsula (MacDonald and Opdyke, 1972).

The Santa Marta batholith records additional exhumation phases at ca. 24 and 14Ma, contrasting with the limited exhumation record in the Parashi stock after 24Ma and the contemporaneous basin deepening in the Guajira basins (Lockwood, 1966; Vence, 2008). Between 25.8 and 9.5Ma there is evidence for an increase in convergence rates between North and South America, with values of 9.6-2.1mm/y (Müeller et al., 1999). The two periods of exhumation recorded in Santa Marta may have been triggered by this geodynamic configuration. Additional tectonic controls that favor exhumation during these periods include a Late Oligocene increase in the convergence rate between the Farallon plate and the western margin of South America (Pardo-Casas and Molnar, 1987), which was responsible for the northeastern migration of the Northern Andean blocks (including the Maracaibo block) in a fashion similar to what is seen today by GPS measurement (Trenkamp et al., 2002). Within this scenario the northern Andean blocks are pushed to the North to override the thick Caribbean plate, facilitating uplift in a way as has been argued for several segments of the Central and Southern Andes (Silver et al., 1998; Oncken et al., 2006; Kay and Coira, 2009; Ramos, 2009).

The difference in the post-Oligocene exhumation behavior between the Santa Marta and Guajira regions is also probably related to the differences between the degree of convergence obliquity. The Guajira region is apparently influenced by more oblique convergence relations than the Santa Marta region (Fig. 7C).

REGIONAL CORRELATIONS

The Santa Marta massif, the Guajira Serranías, the Perijá Range, the Venezuelan Andes and offshore and onshore bounding basins are part of the Maracaibo block (Case et al., 1984). Although previous fission track data on the adjacent Perijá range by Kohn et al. (1984) are not precise due to the acquisition technique based on the population method and the absence of track length data (reviews on Lisker et al., 2009), the correlation of the results with tectonostratigraphic analysis (Kellogg, 1984) suggest that the Sierra de Perijá experienced uplift phases during the Early and Middle Eocene, Late Oligocene and Pliocene.

Recent structural analysis of the Paleogene Ranchería basin in the southeast foothills of the Santa Marta massif also revealed the existence of a major post–50Ma shortening event (Montes et al., 2010), while apatite fission track analyses on Cretaceous sedimentary rocks of the southwestern flank of the Perijá Massif (Fig. 1A) have shown a major Miocene (ca. 12Ma) event (Hernández and Jaramillo, 2009).

The Valle Inferior of the Magdalena and Guajira basins that surround the Santa Marta and Guajira uplifted regions also record major Late Eocene–Early Oligocene, Late Oligocene–Early Miocene and Late Miocene sedimentary hiatuses (Rincón et al., 2007). Published

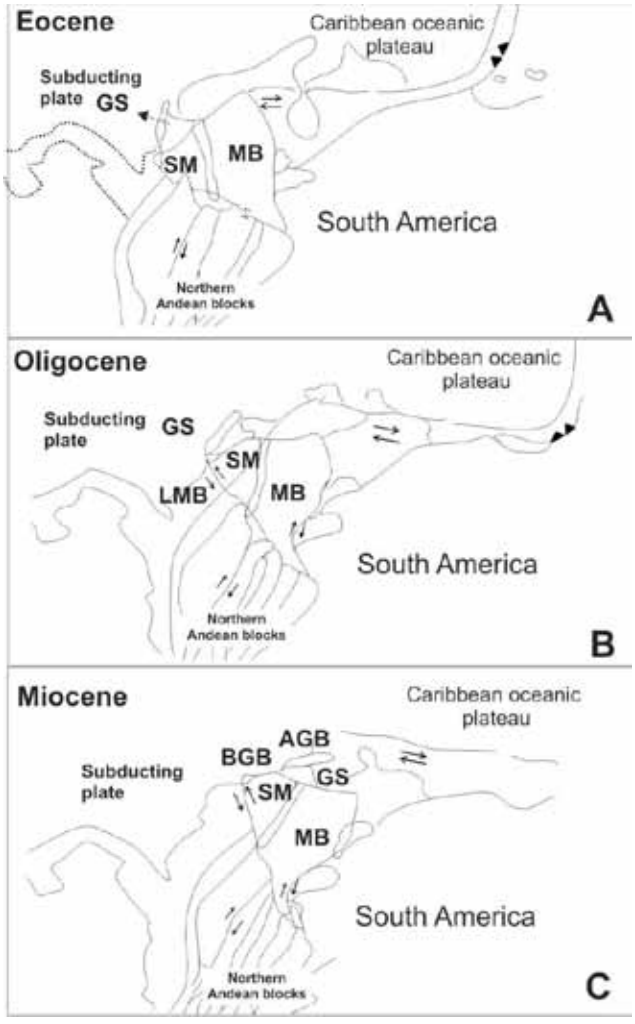

FIGURE 7 | **Cenozoic paleogeographic reconstructions of northwestern South America-Caribbean region (modified from Montes et al., 2005; 2009; Pindell and Keenan, 2009). A) Paleogene, B) Oligocene, C) Miocene-Present. See text for details. SM: Santa Marta Massif, GS: Guajira Serranía, AGB: Alta Guajira Basin, BGB: Baja Guajira Basin, LMB: Lower Magdalena Valley Basin, MB: Maracaibo Block.**

thermochronological data for the Mérida Andes of Venezuela have also shown the existence of three distinct cooling/exhumation events at ca. 2-4Ma, 6-8Ma and 17-20Ma (Kohn et al., 1984; Bermúdez et al., 2010). Similarly, the evolution of the Leeward Antilles records several phases of transtension, block rotation and a major uplift in the Late Miocene (Beardsley and Avé Lallemant, 2007; Gorney et al., 2007).

All these data indicate that the Eocene to Miocene exhumation events found in the Santa Marta and Guajira regions have affected the entire Maracaibo block. Although collision of oceanic domains with the South American margin may be responsible for some of the Late Oligocene and Miocene exhumation and deformational events of the northern Andes (Spikings et al., 2001, 2005; Parra et al., 2009; Restrepo-Moreno et al., 2009) and the Circum-Caribbean region (Sisson et al., 2008), major changes in oceanic-continent convergence relations and variations in thickness of the subducted oceanic crust seem to be the main control for exhumation and uplift in some of these orogens where evidence for collision is null (Pardo-Casas and Molnar, 1987; Silver et al., 1998; Spikings et al., 2001).

CONCLUSIONS

U-Th/He zircon and apatite thermochronological constraints and geological considerations from the Paleogene Santa Marta batholith and the Parashi stock have shown the existence of distinct Oligocene (ca. 35-24Ma) and Miocene (ca. 15-10Ma) exhumation pulses in the northern Colombian Caribbean region. Plate tectonic analysis suggests that the major controls for pre-Late Eocene events are the collision between the Caribbean plate margin and the South American continent in the Late Cretaceous–Early Paleocene and the new subduction zone that was initiated in the Early Eocene. In contrast, the post-Late Eocene events may be correlated to major changes in the rate and vector of convergence between the North and South American plates, the associated underthrusting of the buoyant Caribbean plate, and the northwestern fast overriding of the continent over the oceanic plate.

Differences in the exhumation patterns of the Eocene Santa Marta and Guajira granitoids are related to the separation of these massifs from a former continuous margin, and the formation of different transtensional basins in northeastern Colombia.

These events are temporally correlatable with other Andean and Circum-Caribbean areas and reflect the major plate tectonic reorganizations during the Cenozoic and their influence in regional orogeny.

ACKNOWLEDGMENTS

ECOPETROL-ICP, INGEOMINAS and INVEMAR are acknowledged for the support given to A. Cardona during his participation in the Sierra Nevada de Santa Marta geological project, including access to sample collections. Diego Morata and an anonymous reviewer are acknowledged for their suggestions and reviews that enormously improved the manuscript. Sergio Restrepo is acknowledged for his valuable suggestions. Field work in the Guajira Region and U-Th/He analyses received support from the Fundación para el Apoyo de la Investigación y la Cultura del Banco de la República de Colombia (project 2289), and the Universidad Nacional de Colombia DIME Grant 30805975. Funding for the LaserChron Center was provided by the NSF EAR-0443387. Scientific support by C. Jaramillo is enormously appreciated. C. Bustamante and S. Zapata are acknowledged for helping with the data organization and sample collection. A. García-Casco is acknowledged for continuous discussions and encouragement. This is a contribution to the IGCP 546: "Subduction zones of the Caribbean".

REFERENCES

Avé Lallemant, H.G., 1997. Transpression, displacement partitioning, and exhumation in the eastern Caribbean/South American plate boundary zone. Tectonics, 16, 272-289.

Ayala-Calvo, C., Bayona, G., Ojeda-Marulanda, Cardona, A., Valencia, V., Padrón, C.E., Yoris, F., Mesa-Salamanca, J., García, A., 2010. Stratigraphy and provenance of Campanian-Paleogene units in Cesar sub-basin: contributions to the regional tectonic evolution. Geología Colombiana, 34, 1-34.

Bayona, G., Lamus-Ochoa, F., Cardona, A., Jaramillo, C., Montes, C., Tchegliakova, N., 2007. Procesos orogénicos del Paleoceno para la Cuenca Ranchería (Guajira, Colombia) y áreas adyacentes definidos por análisis de procedencia. Geología Colombiana, 32, 21-46.

Bayona, G., Jimenez, G., Silva, C., Cardona, A., Montes, C., Roncancio, J., 2010. Paleomagnetic data uncovered from Mesozoic units of the Santa Marta massif: constrain for paleogeographic and paleotectonic evolution of the NW corner of the South America plate. Journal of South American Earth Sciences, 29, 817-831.

Beardsley, A.G., Avé-Lallemant, H.G., 2007. Oblique collision and accretion of the Netherlands Leeward Antilles to South America. Tectonics, 26, TC2009, 16pp. doi: 10.1029/2006TC002028

Bermúdez, M.A., Kohn, B.P., van der Beek, P.A., Bernet, M., O'Sullivan, P.B., Shagam, R., 2010. Spatial and temporal patterns of exhumation across the Venezuelan

Andes: Implications for Cenozoic Caribbean geodynamics. Tectonics, 29, TC5009. doi: 10.1029/2009TC002635

Bernet, M., Spiegel, C., 2004. Introduction: Detrital thermochronology. In: Bernet, M., Spiegel, C. (eds.). Detrital Thermochronology: Provenance analysis, Exhumation and Landscape Evolution of Mountain Belts. Geological Society of America Special Publication, 378, 1-8.

Burke, K., 1988. Tectonic evolution of the Caribbean. Annual Reviews on Earth and Planetary Science, 16, 201-230.

Burke, K., Cooper, C., Dewey, J.F., Mann, P., Pindell, J.L., 1984. Caribbean tectonics and relative motions. In: Bonini, W.E., Hargraves, R.B., Shagam, R., (eds.). The Caribbean–South American plate boundary and regional tectonics. Geological Society of America Memoir, 162, 31-63.

Bustamante, C., Cardona, A., Saldarriaga, M., García-Casco, A., Valencia, V., Weber, M., 2009. Metamorfismo de los esquistos verdes y anfibolitas pertenecientes a los Esquistos de Santa Marta, Sierra Nevada de Santa Marta (Colombia): ¿registro de la colisión entre el Arco Caribe y la margen Suramericana? Boletín de Ciencias de la Tierra, 27, 7-24.

Brown, R.W., Summerfield, M.A., 1997. Some uncertainties in the derivation of rates of denudation from thermochronologic data. Earth Surface Process and Landforms, 22, 239-248.

Cardona, A., Weber, M., Cordani, U., Wilson, R., Gomez, J., 2007. Evolución tectono-magmática de las rocas máficas-ultramáficas del Cabo de la Vela y el Stock de Parashi, Península de la Guajira: registro de la evolución orogénica Cretácica-Eocena del norte de Suramérica y el Caribe. Bucaramanga, August 14-17, XI Congreso Colombiano de Geología, CD with Abstracts, 1-7.

Cardona, A., García-Casco, A., Valencia, V., Weber, M., Pepper, M., 2009. Coastal Cretaceous Metamorphic Complexes of the Sierra Nevada de Santa Marta: a Record of Collision and Subduction. Havana (Cuba), March 13–25, Workshop "Subduction Zones of the Caribbean". Available at: http://www.ugr.es/~agcasco/igcp546/

Cardona, A., Duque, J.F., Ruiz, J., Valencia, V., Bayona, G., Jaramillo, C., Ojeda, G., Orozco, M.T., 2008. Geochronology and tectonic implications of granitoids rocks from the northwestern Sierra Nevada de Santa Marta and surrounding basins, northeastern Colombia: Late Cretaceous to Paleogene convergence, accretion and subduction interactions between the Caribbean and South American plates. 24th–28th March 2008, Santo Domingo (Dominican Republic), Abstract Volume of the 18th Caribbean Geological Conference, 24-25.

Cardona, A., Valencia, V., Bustamante, C., Garcia-Casco, A., Ojeda, G., Ruiz, J., Saldarriaga, M., Weber, M., 2010a. Tectonomagmatic setting and provenance of the Santa Marta Schists, Northern Colombia: insights on the growth and approach of Cretaceous Caribbean Oceanic Terranes to the South American continent. Journal of South American Earth Sciences, 29, 784-804.

Cardona, A., Chew, D., Valencia, V.A., Bayona, G., Miskovic, A., Ibañez-Mejia, M., 2010b. Grenvillian remnants in the Northern Andes: Rodinian and Phanerozoic paleogeographic perspectives. Journal of South American Earth Sciences, 29, 784-804.

Cardona, A., Valencia, V., Garzón, A., Montes, G., Ojeda, G., Ruiz, J., Weber, M., 2010c. Permian to Triassic I to S-type magmatic switch in the northeast Sierra Nevada de Santa Marta and adjacent regions, Colombian Caribbean: Tectonic setting and implications within Pangea paleogeography. Journal of South American Earth Sciences, 29, 772-783.

Cardona-Molina, A., Cordani, U., MacDonald, W., 2006. Tectonic correlations of pre-Mesozoic crust from the northern termination of the Colombian Andes, Caribbean region. Journal of South American Earth Sciences, 21, 337-354.

Case, I.E., MacDonald, W., 1973. Gravity Anomalies and Crustal Structure in Northern Colombia. Geological Society of America Bulletin, 84, 2905-2916.

Case, J., Holcombe, T.L., Martin, R.G., 1984. Map of geologic provinces in the Caribbean region. In: Bonini, W.E., Hargraves, R.B., Shagam, R., (eds.). The Caribbean–South American plate boundary and regional tectonics. In: Bonini, W.E., Hargraves, R.B., Shagam, R., (eds.). The Caribbean–South American plate boundary and regional tectonics. Geological Society of America Memoir, 162, 1-31.

Cawood, P.A., Kröner, A., Collins, W.J., Kusky, T.D., Mooney, W.D., Windley, B.F., 2009. Accretionary orogens through Earth history. In: Cawood, P.A., Kröner, A. (eds.). Earth accretionary systems in space and time. London, Geological Society, 318 (Special Publications), 1-36.

Cerón, J., Kellogg, J., Ojeda, G.Y., 2007. Basement configuration of the northwestern South America-Caribbean margin from recent geophysical data. Ciencia, Tecnología y Futuro, 3, 25-49.

Cerón-Abril, J., 2008. Crustal structure of the Colombian Caribbean basin and margins. University of South Carolina. PhD Thesis. 165pp.

Cloos, M., 1993. Lithospheric buoyancy and collisional orogenesis: Subduction of oceanic plateaus, continental margins, island arcs, spreading ridges, and seamounts. Geological Society of America Bulletin, 105, 715-737.

Colgan, J.P., Shuster, D.L., Reiners, P.W., 2008. Two-phase Neogene extension in the northwestern Basin and Range recorded in a single thermochronology sample. Geology, 36, 631-634.

Colmenares, L., Zoback, M.D., 2003. Stress field and seismotectonics of northern South America. Geology, 31, 721-724.

Cordani, U.G., Cardona, A., Jimenez, D., Liu, D., Nutman, A.P., 2005. Geochronology of Proterozoic basement inliers from the Colombian Andes: tectonic history of remnants from a fragmented Grenville belt. In: Vaughan, A.P.M., Leat, P.T., Pankhurst, R.J. (eds.). Terrane Processes at the Margins of Gondwana. Geological Society of London, 246 (Special Publication), 329-346.

Cortés, M., Angelier, J., Colletta, B., 2005. Paleostress evolution of the northern Andes (Eastern Cordillera of Colombia):

Implications on plate kinematics of the South Caribbean region. Tectonics, 24(1), doi: 10.1029/2003TC001551

Cross, T.A., Pilger, R.H., 1982. Controls on subduction gemetry, location of magmatic arcs, and tectonics of arc and back-arc regions. Geological Society of America Bullettin, 93, 545-562.

Cruz, L., Fayon, A., Teyssier, Ch., Weber, J., 2007. Exhumation and deformation processes in transpressional orogens: The Paria Peninsula, SE Caribbean–South American plate boundary. In: Till, A.B., Roeske, S.M., Sample, J.C., Foster, D. (eds.). Exhumation associated with strike-slip systems. Geological Society of America, 434 (Special Paper), 149-165.

DeCelles, P.G., Ducea, M.N., Kapp, P., Zandt, G., 2009. Cyclicity in Cordilleran orogenic systems. Nature Geoscience, 2, 251-257.

Doolan, B.L., 1971. Structure and metamorphism of the Santa Marta area, Colombia, South America. Ph.D. Thesis. Binghamton (New York), New York State University, 200pp.

Dimate, C., Rivera, L., Taboada, A., Delouis, B., Osorio, A., Jimenez, E., Fuenzalida, A., Cisternas, A., Gomez, I., 2003. The 19 January 1995 Tauramena (Colombia) earthquake: geometry and stress regime. Tectonophysics, 363, 159-180.

Duque, J., Orozco, M.T., Cardona, A., Ferrari, L., Solari, L., 2009. Geoquímica y geocronología (U/Pb y Ar/Ar) de las rocas Paleoceno-Eoceno en la Sierra Nevada de Santa Marta y sus relaciones con la tectónica del Caribe y el arco magmático Circum-Caribeño. Paipa, XII Colombian Geological Congress, September, CD with abstracts, 7-11.

Duque-Caro, H., 1979, Major structural elements and evolution of northwestern Colombia. In: Watkins, J.S., Montadert, L., Dickerson, P.W. (eds.). Geological and geophysical investigations of continental margins. American Association of Petroleum Geologists, 29 (Memoir), 329-351.

Duque-Caro, H., 1984. Structural Style, diapirism and accretionary episodes of the Sinu-San Jacinto terrane, southwestern Caribbean borderland. In: Bonini, W.E., Hargraves, R.B., Shagam, R., (eds.). The Caribbean–South American plate boundary and regional tectonics. Geological Society of America Memoir, 162, 303-316.

Espurt, N., Funiciello, F., Martinod, J., Guillaume, B., Regard, V., Faccenna, C., Brusset, S., 2008. Flat subduction dynamics and deformation of the South American plate: Insights from analog modeling. Tectonics, 27, TC3011. doi:10.1029/2007TC002175

Farley, K.A., Wolf, R.A., Silver, L.T., 1996. The effects of long alpha-stopping distances on (U-Th)/He ages. Geochimica et Cosmochimica Acta, 60, 4223-4229.

Farley, K.A., 2000, Helium diffusion from apatite: General behavior as illustrated by Durango fluorapatite. Journal of Geophysical Research, 105, 2903-2914. doi:10.1029/1999JB900348

Farley, K.A., 2002. (U-Th)/He dating: techniques, calibrations, and applications. Reviews in Mineral and Geochemistry, 47, 819-844.

Fitzgerald, P.G., Baldwin, S.L., Webb, L.E., O'Sullivan, P.B., 2006. Interpretation of (U-Th)/He single grain ages from slowly cooled crustal terranes: A case study from the Transantarctic Mountains of southern Victoria Land. Chemical Geology, 225, 91-120.

Gehrels, G., Valencia, V., Ruiz, J., 2008. Enhanced precision, accuracy, efficiency, and spatial resolution of U-Pb ages by laser ablation-multicollector-inductively coupled plasma mass spectrometry. Geochemistry, Geophysics, Geosystems, 9, Q03017. doi: 10.1029/2007GC001805

Gerya, T., Fossati, D., Cantieni, C., Seward, D., 2009. Dynamic effects of aseismic ridge subduction: numerical modeling. European Journal of Mineralogy, 21, 649-661.

Glazner, A.F., Bartley, J.M., Coleman, D.S., Gray, W., Taylor, R.Z., 2004. Are plutons assembled over millions of years by amalgamation from small magma chambers? GSA Today, 14, 4-11.

Gómez, E., Jordan, T., Allmendinger, R.W., Hegarty, K., Kelley, S., 2005. Syntectonic Cenozoic sedimentation in the northern middle Magdalena Valley Basin of Colombia and implications for exhumation of the Northern Andes. Geological Society of America Bulletin, 117, 547-569.

Gorney, D., Escalona, A., Mann, P., Magnani, M.B., and the BOLIVAR Study Group, 2007. Chronology of Cenozoic tectonic events in western Venezuela and the Leeward Antilles based on integration of offshore seismic reflection data and onland geology. American Association of Petroleum Geologists Bullettin, 91, 653-684.

Gorczyk, W., Willner, A.P., Gerya, T.V., Connolly, J.A.D., Burg, J.-P., 2007. Physical controls of magmatic productivity at Pacific-type convergent margins: Numerical modeling. Physics of the Earth and Planetary Interiors, 163, 209-232.

Gutsher, M-A, 2002. Andean subduction styles and their effect on thermal structure and intraplate coupling. Journal of South American Earth Sciences, 15, 3-10.

Guzmán, G., 2007, Stratigraphy and sedimentary environment and implicationsin the Plato basin and the San Jacinto belt, northwestern Colombia. Ph.D.Thesis. Belgium, University of Liège, 275pp.

Hall, R., 2002. Cenozoic geological and plate tectonic evolution of SE Asia and the SW Pacific: computer-based reconstructions, model and animations. Journal of Asian Earth Sciences, 20, 353-431.

Hernández, O., Jaramillo, J.M., 2009. Reconstrucción de la historia termal en los sectores de Luruaco y Cerro Cansona–cuenca del Sinú-San Jacinto y en el piedemonte occidental de la Serranía del Perijá entre Codazzi y la Jagua de Ibirico–cuenca de Cesar-Ranchería. Informe Final Cuenca Cesar-Ranchería. Agencia Nacional de Hidrocarburos (Bogotá), 58pp.

Hourigan, J.K., Reiners, P.W., Brandon, M.T., 2005. U-Th zonation-dependent alpha-ejection in (U-Th)/He chronometry. Geochimica et Cosmochimica Acta, 69, 3349-3365.

House, M.A., Farley, K.A., Kohn, B.P., 1999. An empirical test of helium diffusion in apatite: borehole data from the Otway Basin, Australia. Earth and Planetary Science Letters, 170, 463-474.

House, M.A, Farley, K.A., Stockli, D.F., 2000. Helium chronometry of apatite and titanite using Nd-YAG laser heating. Earth and Planetary Science Letters, 183, 365-368.

Hughes, R.A., Pilatasig, L.F., 2002. Cretaceous and Tertiary terrane accretion in the Cordillera Occidental of the Andes of Ecuador. Tectonophysics, 345, 29-48.

Jaillard, E., Bengtson, P., Ordoñez, M., Vaca, W., Dhondt, A., Suarez, J., Toro, J., 2008. Sedimentary record of terminal Cretaceous accretions in Ecuador: The Yunguilla Group in the Cuenca area. Journal of South American Earth Sciences, 25, 133-144.

Jaillard, E., Lapierre, H., Ordoñez, M., Toro Álava, J., Amórtegui, A., Vanmelle, J., 2010. Accreted oceanic terranes in Ecuador: southern edge of the Caribbean plate? In: James, K.H., Lorente, M.A., Pindell, J. (eds.). The Origin and Evolution of the Caribbean Plate. Geological Society of London, 328 (Special Publication), 469-485.

Jarrard, R.D., 1986. Relations among subduction parameters. Reviews of Geophysics, 24, 217-284.

Kay, S.M., Coira, B.L., 2009. Shallowing and steepening subduction zones, continental lithosphere loss, magmatism and crystal flow under the Central Andean Altiplano Puna Plateau. In: Kay, S.M., Ramos, V.A., Dickinson, W.D. (eds.). Backbone of the Americas: Shallow Subduction, Plateau Uplift, and Ridge and Terrane Collision. Geological Society of America, 204 (Memoir), 229-260.

Kennan, L., Pindell, J., 2009. Dextral shear, terrane accretion and basin formation in the Northen Andes: best explained by interaction with a Pacific-derived Caribbean Plate?. In: James, K.H., Lorente, M.A., Pindell, J. (eds.). The Origin and Evolution of the Caribbean Plate. Geological Society of London, 328 (Special Publication), 487-532.

Kellogg, J.N., Bonini, W.E., 1982. Subduction of the Caribbean plate and basement uplifts in the overriding South American plate. Tectonics, 1, 251-276.

Kellogg, J.N., 1984. Cenozoic tectonic history of the Sierra de Perija, Venezuela-Colombia, and adjacent basins. In: Bonini, W.E., Hargraves, R.B., Shagam, R., (eds.). The Caribbean–South American plate boundary and regional tectonics. Geological Society of America Memoir, 162, 239-261.

Kellogg, J.N., Vega, V., 1995. Tectonic development of Panama, Costa Rica, and the Colombian Andes: Constraints from Global Positioning System geodetic studies and gravity. In: Mann, P., Kolarsky, R.A. (eds.). Geologic and Tectonic Development of the Caribbean plate boundary southern Central America. Geological Society of America, 295 (Special Paper), 75-90.

Kerr, A.C., Marriner, G.F., Tarney, J., Nivia, A., Saunders, A.D., Thirlwall, M.F., Sinton, C.W., 1997. Cretaceous basaltic terranes in western Colombia: Elemental, chronological and Sr-Nd constraints on petrogenesis. Journal of Petrology, 38, 677-702.

Kerr, A.C., White, R.V., Thompson, P.M.E., Tarney, J., Saunders, A.D., 2003. No oceanic plateau–no Caribbean Plate? The seminal role of an oceanic plateau in Caribbean plate evolution. In: Bartolini, C., Buffler, R.T., Blickwede, J. (eds.). The Gulf of Mexico and Caribbean Region: Hydrocarbon Habitats, Basin Formation and Plate Tectonics. American Association of Petroleum Geologists, 79 (Memoirs), 126-168.

Kohn, B., Shagam, R., Banks, P., Burkley, L., 1984. Mesozoic–Pleistocene fission track ages on rocks of the Venezuelan Andes and their tectonic implications. In: Bonini, W.E., Hargraves, R.B., Shagam, R., (eds.). The Caribbean–South American plate boundary and regional tectonics. Geological Society of America Memoir, 162, 365-384.

Leake, B.E., Woolley, A.R., Arps, C.E.S., Birch, W.D., Gilbert, M.C., Grice, J.D., Hawthorne, F.C., Kato, A., Kisch, H.J., Krivovichev, V.G., Linthout, K., Laird, J., Mandarino, J.A., Maresch, W.V., Nickel, E.H., Rock, N.M.S., Schumacher, J.C., Smith, D.C., Stephenson, N.C.N., Ungaretti, L., Whittaker, E.J.W., Youzh, G., 1997. Nomenclature of amphiboles: report of the Subcommittee on Amphiboles of the International Mineralogical Association, Commission on New Minerals and Mineral Names. Canadian Mineralogist, 35, 219-246.

Lisker, F., Ventura, B., Glasmacher, U.A., 2009. Apatite thermochronology in modern geology. In: Lisker, F., Ventura, B., Glasmacher, U.A. (eds.). Thermochronological Methods: From Palaeotemperature Constraints to Landscape Evolution Models. Geological Society of London, 324 (Special Publications), 1-23.

Lockwood, J.P., 1966. Geology of the Serranía de Jarara area, Guajira Península, Colombia. Ph.D. Thesis. Princeton, Princeton University, 237pp.

López, C., Ojeda, G., 2006. Heat flow in the Colombian Caribbean from the bottom simulating reflector (BSR). Ciencia Tecnología &. Futuro (C.T.F.), 3, 29-39.

Ludwig, K.R., 2003, User's Manual for Isoplot 3.00. Berkeley, CA, Berkeley Geochronology Center, 70pp.

Ludwig, K.R., Mundil, R., 2003. Extracting reliable U-Pb ages and errors from complex populations of zircons from Phanerozoic tuffs. Geochimica et Cosmochimica Acta, 66, 463. doi: 10.1016/S0016-7037(01)00786-4

Lugo, J., Mann, P., 1995. Jurassic-Eocene tectonic evolution of Maracaibo Basin, Venezuela. In: Tankard, A., Suarez, R., Welsink, H. (eds.). Petroleum Basins of South America. American Association of Petroleum Geologists, 62 (Memoir), 699-725.

Luzieux, L.D.A., Heller, F., Spikings, R., Vallejo, C.F., Winkler, W., 2006. Origin and Cretaceous tectonic history of the coastal Ecuadorian forearc between 1°S-4°S: Paleomagnetic, radiometric and fossil evidence. Earth and Planetary Science Letters, 249, 400-414.

Macellari, C., 1995, Cenozoic sedimentation and tectonics of the southwestern Caribbean pull-apart basin, Venezuela and Colombia. In: Tankard, A., Suarez, S., Welsink, H. (eds.). Petroleum basins of South America. American Association of Petroleum Geologists, 62 (Memoir), 757-780.

MacDonald, W.D., Doolan, B.L., Cordani, U.G., 1971. Cretaceous–Early Tertiary metamorphic K–Ar age values from the South Caribbean. Geological Society of America Bulletin, 82, 1381-1388.

MacDonald, W., Opdyke, N.D., 1972. Tectonic rotations suggested by paleomagnetic results from northern Colombia, South America. Journal of Geophysical Research, 77, 5720-5730.

Malavé, G., Suarez, G., 1995. Intermediate-depth seismicity in northern Colombia and western Venezuela and its relationship to Caribbean Plate subduction. Tectonics, 14, 617-628.

Mancktelow, N., Grasemann, B., 1997. Time-dependent effects of heat advection and topography on cooling histories during erosion. Tectonophysics, 270, 167-195.

Martínez, L.F., 2008. Metamorfismo de contacto y emplazamiento del Stock de Parashi en la Serranía de Jarara, Alta Guajira Colombia. Degree Thesis. Sede Bogotá, Universidad Nacional, 22pp.

Mauffret, A., Leroy, S., 1997. Seismic stratigraphy and structure of the Caribbean igneous province. Tectonophysics, 283, 61-104.

McDougall, I., Harrison, T.M., 1999. Geochronology and thermochronology by the Ar/Ar method. Oxford, University Press, 269pp.

McDowell, F.W., McIntosh, W.C., Farley, K.A., 2005. A precise Ar-40-Ar-39 reference age for the Durango apatite (U-Th)/He and fission-track dating standard. Chemical Geology, 214, 249-263.

Mejía, P., Santa, M., Ordóñez, O., Pimentel., M., 2008. Consideraciones petrográficas, geoquímicas y geocronológicas de la parte occidental del Batolito de Santa Marta. Revista Dyna, 155, 223-236.

Miller, M.S., Levander, A., Niu, F., Li, A., 2009. Upper mantle structure beneath the Caribbean–South American plate boundary from surface wave tomography. Journal of Geophysical Research, 114, B01312. doi:10.1029/2007JB005507

Montes, C., Hatcher, R.D., Restrepo-Pace, P., 2005, Tectonic reconstruction of the northern Andean blocks: Oblique convergence and rotations derived from the kinematics of the Piedras-Girardot area, Colombia. Tectonophysics, 399, 221-250.

Montes, C., Guzmán, G., Bayona, G., Cardona, A., Valencia, V., 2010. Clockwise Rotation of the Santa Marta Massif and Simultaneous Paleogene to Neogene Deformation of the Plato-San Jorge and Cesar-Ranchería Basins. Journal of South American Earth Sciences, 29, 832-848.

Muessig, K.W. 1984. Structure and Cenozoic tectonics of the Falcón Basin, Venezuela, and adjacent areas. In: Bonini, W.E., Hargraves, R.B., Shagam, R. (eds.). The Caribbean–South American plate boundary and regional tectonics. Geological Society of America Memoir, 162, 217-230.

Müeller, R.D., Royer, J-Y, Cande, S.C., Roest, W.R., Maschenkov, S., 1999. New Constraints on Caribbean Plate Tectonic Evolution Caribbean Basins included in the series. Elsevier Science, Sedimentary Basins of the World, 4, 33-59.

Oncken, O., Hindle, D., Kley, J., Elger, K., Victor, P., Schemmann, K., 2006. Deformation of the central Andean plate system - Facts, fiction, and constraints for plateau models. In: Oncken, O., Chong, G., Franz, G., Giese, P., Götze, H.J., Ramos, V.A., Strecker, M.R., Wigger, P. (eds.). The Andes-Active subduction orogeny. Berlin-Heidelberg, Springer, 3-27.

Parada, M.A., Féraud, G., Fuentes, F., Aguirre, L., Morata, D., Larrondo, P., 2005. Ages and cooling history of the Early Cretaceous Caleu pluton: testimony of a switch from a rifted to a compressional continental margin in central Chile. Journal of the Geological Society of London, 205, 273-287.

Pardo-Casas, F., Molnar, P., 1987. Relative motion of the Nazca (Farallon) and South American plates since Late Cretaceous time. Tectonics, 6, 233-248.

Parra M., Mora, A., Sobel, E.R., Strecker, M.R., González, R., 2009. Episodic orogenic front migration in the northern Andes: Constraints from low-temperature thermochronology in the Eastern Cordillera, Colombia. Tectonics, 28, TC4004. doi:10.1029/2008TC002423

Perez, O.J., Bilham, R., Bendick, R., Velandia, J.R., Hernandez, N., Moncayo, C., Hoyer, M., Kozuch, M., 2001. Velocity field across the southern Caribbean plate boundary and estimates of Caribbean/South-American Plate motion using GPS geodesy 1994-2000. Geophysical Research Letters, 28, 2987-2990.

Pérez de Armas, J., 2005. Tectonic and thermal history of the western Serranía del Interior foreland fold and thrust belt and Guárico basin, north-central Venezuela: Implication of new apatite fission-track analysis and seismic interpretations. In: Avé Lallament, H.G., Sisson, V.B. (eds.). Caribbean–South American Plate Interactions, Venezuela. Geological Society of America 394 (Special Paper), 271-314.

Pilger, R.H., 1984. Cenozoic plate kinematics, subduction and magmatism: South American Andes. Journal Geological Society of London, 141, 793-802.

Pindell, J.L., 1993, Evolution of the Gulf of Mexico and the Caribbean: An Introduction. In: Donovan, S.K., Jackson, T.A. (eds.). University of the West Indies Publisher's Association Caribbean Geology, 13-39.

Pindell, J.L., Cande, S.C., Pitman, III W.C., Rowley, D.B., Dewey, J.F., LaBrecque, J., Haxby, W., 1988. A plate-kinematic framework for models of Caribbean evolution. Tectonophysics, 155, 121-138.

Pindell, J.L., Higgs, R., Dewey, J.F., 1998. Cenozoic palinspastic reconstruction, paleogeographic evolution, and hydrocarbon setting of the northern margin of South America. In: Pindell, J.L., Drake, C.L. (eds.). Paleogeographic Evolution and Non-glacial Eustasy, northern South America. Society for Sedimentary Geology (SEPM), 58 (Special Publication), 45-86.

Pindell, J., Kennan, L., Maresch, W.V., Stasnek, K.-P., Draper, G., Higgs, R., 2005. Plate kinematic and crustal dynamics of circum-Caribbean arc-continent interactions: Tectonic controls on basin development in the Proto-Caribbean margins. In: Avé Lallemant, H.G., Sisson, V.B. (eds.). Caribbean–South American plate interactions, Venezuela. Geological Society of America, 394 (Special Paper), 7-52.

Pindell, J., Kennan, L., 2009. Tectonic evolution of the Gulf of Mexico, Caribbean and northern South America in the mantle reference frame: an update. In: James, K.H., Lorente, M.A., Pindell, J. (eds.). The Origin and Evolution of the Caribbean Plate. Geological Society of London, 328 (Special Publications), 1-56.

Ramos, V.A., 2009. Anatomy and global context of the Andes: Main geologic features and the Andean orogenic cycle. In: Kay, S.M., Ramos, V.A., Dickinson, W.D. (eds.). Backbone of the Americas: Shallow Subduction, Plateau Uplift, and Ridge and Terrane Collision. Geological Society of America, 204 (Memoir), 31-66.

Reiners, P.W., 2005. Zircon (U-Th)/He Thermochronometry. In: Reiners, P.W., Ehlers, T.A. (eds.). Thermochronology. Reviews in Mineralogy and Geochemistry, 58, 151-176.

Reiners, P.W., Farley, K.A., Hickes, H.J., 2002. He diffusion and (U-Th)/He thermochronometry of zircon: Initial results from Fish Canyon Tuff and Gold Butte, Nevada. Tectonophysics, 349, 297-308.

Restrepo-Moreno, S.A., Foster D.A., Stockli, D.F., Parra-Sánchez, L-N., 2009. Long-term erosion and exhumation of the "Altiplano Antioqueño", Northern Andes (Colombia) from apatite (U-Th)/He thermochronology. Earth and Planetary Science Letters, 278, 1-2.

Rincón, D., Arenas, J.E., Cuartas, C.H., Cárdenas, A.L., Molinares, C.E., Caicedo, C., Jaramillo, C., 2007. Eocene-Pliocene planktonic foraminifera biostratigraphy from the continental margin of the southwest Caribbean. Stratigraphy, 4, 261-311.

Ring, U., Brandon, M.T., Willett, S., Lister, G., 1999. Exhumation processes. In: Ring, U., Brandon, M.T., Willett, S., Lister, G. (eds.). Exhumation Processes: Normal Faulting, Ductile Flow, and Erosion. Geological Society of London, 154 (Special Publication), 1-27.

Saint Blanquat, M., Tikoff, B., Teyssier, C., Vigneresse, J.L., 1998. Transpressional kinematics and magmatic arcs. In: Holdsworth, R.E., Strachan, R.A., Dewey, J.F., (eds.). Continental Transpressional and Transtensional Tectonics. Geological Society of London, 135 (Special Publication), 327-341.

Schmidt, M.W., 1992. Amphibole composition in tonalite as a function of pressure: An experimental calibration of the Al-in-hornblende barometer. Contributions to Mineralogy and Petrology, 110, 304-310.

Silver, P.G., Russo, R.M., Lithgow-Bertelloni, C., 1998. Coupling of South American and African plate motion and plate deformation. Science, 279, 60-63.

Sisson, V.B., Avé Lallemant, H.G., Sorensen, S.S., 2008. Correlation of Eocene-Oligocene Exhumation around the Caribbean. Venezuela, Dominican Republic, Honduras, and Guatemala, Geological Society of America, Abstracts, 292-298.

Sobolev, S.V., Babyko, A.Y., 2005. What drives orogeny in the Andes? Geology, 33, 617-620.

Spikings, R.A., Seward, D., Winkler, W., Ruiz, G., 2000. Low temperature thermochronology of the northern Cordillera Real, Ecuador: tectonic insights from zircon and apatite fission track analysis. Tectonics, 19, 649-668.

Spikings, R.A., Winkler, W., Seward, D., Handler, R., 2001. Along-strike variations in the thermal and tectonic response of the continental Ecuadorian Andes to the collision with heterogeneous oceanic crust. Earth and Planetary Science Letters, 186, 57-73.

Spikings, R.A., Winkler, W., Hughes, R.A., Handler, R., 2005. Thermochronology of Allochthonous Terranes in Ecuador: unraveling the accretionary and post-accretionary history of the Northern Andes. Tectonophysics, 399, 195-220.

Spikings, R., Dungan, M., Foeken, J., Carter, A., Page L., Stuart, F., 2008. Tectonic response of the central Chilean margin (35–38°S) to the collision and subduction of heterogeneous oceanic crust: a thermochronological study. Journal of the Geological Society of London, 165, 941-953.

Spotila, J.A., Farley, K., Sieh, K.E., 1998. Uplift and erosion of the San Bernardino Mountains associated with transpression along the San Andreas fault, California, as constrained by radiogenic helium thermochronometry. Tectonics, 17, 360-378.

Stacey, J.S., Kramers, J.D., 1975, Approximation of terrestrial lead isotope evolution by a two-stage model. Earth and Planetary Science Letters, 26, 207-221.

Steiger, R.H., Jager, E., 1977. Subcommission on geochronology: Convention on the use of decay constants in geo- and cosmochronology. Earth and Planetary Science Letters, 36(3), 359-362.

Stockli, D.F., Farley, K.A., Dumitru, T.A., 2000. Calibration of the (U-Th)/He thermochronometer on an exhumed normal fault block in the White Mountains, eastern California and western Nevada. Geology, 28, 983-986.

Taboada, A, Rivero, L., Fuenzalida, A, Cisternas, A, Philip, H., Bijwaard, H., Olaya, J, Rivera, C., 2000. Geodynamics of the northern Andes: Subduction and intracontinental deformation (Colombia). Tectonics, 19, 787-813.

Thomson, N., 1994. Fission-track analysis and provenance studies in Calabrian Arc sedimentary rocks, southern Italy. Journal of the Geological Society of London, 151, 463-471.

Thompson, A.B., Schulmann, K., Jezek, J., 1997. Thermal evolution and exhumation in obliquely convergent (transpressive) orogens. Tectonophysics, 280, 171-184.

Toto, E.A., Kellogg, J.N., 1992. Structure of the Sinu-San Jacinto fold belt-An active accretionary prism in northern Colombia. Journal of South American Earth Sciences, 5, 211-222.

Trenkamp, R., Kellogg, J.N., Freymueller, J.T., Mora, H.P., 2002. Wide plate margin deformation, southern Central America and northwestern South America, CASA GPS observations. Journal of South American Earth Sciences, 15, 157-171.

Tschanz, C.M., Jimeno, A., Vesga, C., 1969. Geology of the Sierra Nevada de Santa Marta area (Colombia). República de Colombia, Instituto de Investigaciones e Información Geocientífica, Minero–Ambiental y Nuclear, 288pp.

Tschanz, C., Marvin, R., Cruz, J., Mehnert, H., Cebula, E., 1974. Geologic evolution of the Sierra Nevada de Santa Marta. Geological Society of America Bulletin, 85, 273-284.

Vallejo, C., Spikings, R.A., Winkler, W., Luzieux, L., Chew, D., Page, L., 2006. The early interaction between the Caribbean Plateau and the NW South American plate. Terra Nova, 18, 264-269.

Vallejo, C.F., Winkler, W., Spikings, R.A., Luzieux, L.D.A., Heller, F., Bussy, F., 2009. Mode and timing of terrane accretion in the forearc of the Andes in Ecuador. In: Kay, S.M., Ramos, V.A., Dickinson, W.R. (eds.). Backbone of the Americas: Shallow Subduction, Plateau Uplift, and Ridge and Terrane Collision. Geological Society of America Memoir, 204, 197-216.

Van der Hilst, R., Mann, P., 1994. Tectonic implications of tomographic images of subducted lithosphere beneath northwestern South America. Geology, 22, 451-454.

Van der Lelij, R., Spikings, R.A., Kerr, A., Kounov, A., Cosca, M., Chew, D., Villagomez, D., in press. Thermochronology and Tectonics of the Leeward Antilles: evolution of the Southern Caribbean Plate Boundary Zone. Tectonics.

Vence, E.M., 2008. Subsurface structure, stratigraphy, and regional tectonic controls of the Guajira margin of northern Colombia. MSc. Thesis. Austin, The University of Texas, CD ROM.

Von Houne, R., Ranero, C.R., 2009. Neogene collision and deformation of convergent margins along the backbone of the Americas. In: Kay, S.M., Ramos, V.A., Dickinson, W.R., (eds.). Backbone of the Americas: Shallow Subduction, Plateau Uplift, and Ridge and Terrane Collision. Geological Society of America Memoir, 204, 67-84.

Weber, J., Dixon, T., DeMets, C., Ambeh, W., Jansma, P., Mattioli, G., Bilham, R., Saleh, J., Perez, O., 2001. A GPS Estimate of the Relative Motion between the Caribbean and South American Plates, and Geologic Implications for Trinidad and Venezuela. Geology, 29, 75-78.

Weber, M., Cardona, A., Wilson, R., Gómez-Tapias, J., Zapata, G., 2007. Química Mineral de las rocas de alta presión-Facies Eclogita, de la Península de la Guajira, Colombia. Boletín de Geología, 29, 31-39.

Weber, M.B.I., Cardona, A., Paniagua, F., Cordani, U., Sepúlveda, L, Wilson, R., 2009. The Cabo de la Vela mafic-ultramafic complex, Northeastern Colombian Caribbean region–a record of multi stage evolution of a Late Cretaceous intra-oceanic arc. In: James, K.H., Lorente, M.A., Pindell, J. (eds.). The Origin and Evolution of the Caribbean Plate. Geological Society of London, 328 (Special Publication), 549-568.

Weber, M.B., Cardona, A., Valencia, V., García-Casco, A., Tobón, M., Zapata, S., 2010. U/Pb detrital zircon provenance from Late Cretaceous metamorphic units of the Guajira Peninsula, Colombia: tectonic implications on the collision between the Caribbean arc and the South American margin. Journal of South American Earth Sciences, 29, 805-816.

Wipf, M., Zeilinger, G., Seward, D., Schlunegger, F., 2008 Focused subaerial erosion during ridge subduction: impact on the geomorphology in south-central Peru. Terra Nova, 20, 1-10.

Zapata, S., Weber, M., Cardona, A., Valencia, V., Guzmán, G., Tobón, M., in press. Provenance of Oligocene conglomerates and associated sandstone from the Siamaná Formation, Serranía de Jarara, Guajira, Colombia: Implications for Oligocene Caribbean South American Tectonics. Boletín de Ciencias de la Tierra.

Manuscript received November 2010;
revision accepted July 2011;
published Online July 2011.

ELECTRONIC APPENDIX

TABLE I | **Electron microprobe chemical data and pressure calculations from the analyzed amphiboles of the Santa Marta batholith and Parashi stock**

	Santa Marta Batholith																		
Sample	EMC-1	EMC-1	EMC-1	EMC-1	EMC-1	EMC-1	EMC-1	EMC-1	EMC-1	BSM-7A	BSM-7A	BSM-7A	BSM-7A	BSM-7A	BSM-7A	BSM-7A	BSM-7A	BSM-13	BSM-13
Analysis	1	2	3	4	5	7	8	9	10	2	3	4	5	6	7	8	9	1	2
SiO_2	42.00	43.00	43.00	43.00	43.00	44.00	43.00	43.00	42.00	42.64	42.65	43.04	43.43	43.38	41.94	43.07	42.43	44.57	43.62
TiO_2	0.53	0.72	0.85	0.56	0.69	0.88	0.48	0.55	0.98	0.71	0.96	0.95	1.10	0.93	0.92	0.69	1.07	0.99	0.88
Al_2O_3	11.21	10.37	10.66	10.79	10.36	10.45	10.55	11.00	10.58	10.81	11.20	10.83	10.53	10.65	11.52	10.75	11.00	11.33	11.42
FeO	18.54	18.13	17.68	18.28	17.88	17.94	18.04	18.33	18.12	17.85	17.81	17.91	17.49	17.66	17.62	17.74	17.57	17.84	16.95
MnO	0.73	0.74	0.72	0.72	0.73	0.75	0.73	0.71	0.74	0.62	0.59	0.57	0.60	0.60	0.63	0.62	0.64	0.50	0.48
MgO	9.03	9.88	10.18	9.53	9.70	9.79	9.97	9.46	9.68	9.83	10.19	10.16	10.00	10.44	9.55	10.00	10.23	9.90	10.40
CaO	11.70	11.59	11.60	11.52	11.72	11.38	11.61	11.63	11.48	11.81	11.73	11.75	11.66	11.65	11.63	11.52	11.58	11.28	11.69
Na_2O	1.00	1.00	1.00	1.00	1.00	1.00	1.00	1.00	2.00	0.98	1.24	1.27	1.10	1.20	0.95	1.13	1.33	1.56	1.40
K_2O	1.18	0.93	0.85	1.09	0.99	1.04	0.89	1.07	0.93	0.92	1.16	1.08	1.04	0.98	0.88	1.11	1.08	0.94	0.81
Total	95.92	96.37	96.54	96.48	96.07	97.23	96.27	96.76	96.51	95.56	98.66	98.67	98.89	97.71	94.93	97.98	98.98	99.09	98.08
Si	6.407	6.478	6.440	6.482	6.515	6.503	6.559	6.470	6.465	6.497	6.445	6.361	6.422	6.510	6.444	6.359	6.363	6.526	6.456
Al iv	1.593	1.522	1.560	1.518	1.485	1.497	1.441	1.530	1.535	1.503	1.555	1.639	1.578	1.490	1.556	1.641	1.637	1.474	1.544
Al vi	0.423	0.319	0.322	0.399	0.365	0.369	0.395	0.341	0.415	0.324	0.370	0.330	0.326	0.370	0.308	0.418	0.308	0.481	0.448
Ti	0.060	0.082	0.096	0.064	0.078	0.065	0.099	0.054	0.062	0.129	0.082	0.108	0.106	0.124	0.103	0.105	0.121	0.110	0.098
Cr	0.004	0.002	0.002	0.000	0.004	0.004	0.000	0.007	0.006	0.005	0.000	0.002	0.002	0.002	0.007	0.003	0.000	0.000	0.000
Fe^{3+}	0.696	0.826	0.866	0.769	0.667	0.749	0.725	0.868	0.746	0.570	0.735	0.766	0.707	0.607	0.797	0.783	0.773	0.616	0.637
Fe^{2+}	1.669	1.458	1.348	1.536	1.599	1.501	1.511	1.401	1.560	1.621	1.521	1.455	1.527	1.586	1.397	1.451	1.430	1.570	1.461
Mn	0.094	0.094	0.092	0.092	0.094	0.091	0.094	0.093	0.091	0.076	0.079	0.075	0.072	0.077	0.076	0.080	0.081	0.063	0.061
Mg	2.054	2.220	2.274	2.141	2.192	2.221	2.175	2.236	2.121	2.275	2.214	2.264	2.259	2.235	2.311	2.159	2.287	2.161	2.295
Ca	1.912	1.871	1.862	1.861	1.902	1.883	1.817	1.872	1.874	1.903	1.912	1.873	1.879	1.873	1.853	1.890	1.860	1.770	1.854
Na	0.296	0.292	0.290	0.292	0.294	0.293	0.289	0.292	0.292	0.337	0.286	0.358	0.367	0.319	0.345	0.278	0.386	0.443	0.403
K	0.230	0.178	0.162	0.209	0.193	0.185	0.199	0.170	0.206	0.204	0.177	0.220	0.206	0.199	0.186	0.170	0.207	0.176	0.154
Total	17.438	17.341	17.314	17.362	17.389	15.361	15.305	15.334	15.371	15.444	15.375	15.452	15.452	15.391	15.384	15.338	15.454	15.388	15.410
Na (B)	0.088	0.129	0.138	0.139	0.098	0.117	0.183	0.128	0.126	0.097	0.088	0.127	0.121	0.127	0.147	0.110	0.140	0.230	0.146
(Na+K) (A)	0.438	0.341	0.314	0.362	0.389	0.361	0.305	0.334	0.371	0.444	0.375	0.452	0.452	0.391	0.384	0.338	0.454	0.388	0.410
$Mg/(Mg+Fe^2)$	0.552	0.604	0.628	0.582	0.578	0.597	0.590	0.615	0.576	0.584	0.593	0.609	0.597	0.585	0.623	0.598	0.615	0.579	0.611
$Fe^3/(Fe^3+Alvi)$	0.622	0.722	0.729	0.658	0.646	0.670	0.647	0.718	0.643	0.638	0.665	0.699	0.684	0.621	0.721	0.652	0.715	0.561	0.587
Sum of S^2	13	13	13	13	13	13	13	13	13	13	13	13	13	13	13	13	13	13	13
P (Kb)	6.6	5.8	5.9	6.1	5.8	5.7	5.9	6.3	6.0	6.2	6.4	6.1	5.8	5.9	6.8	6.0	6.2	6.3	6.5

TABLE I | **Continued**

	Santa Marta Batholith																		
Sample	BSM-13	BSM-13	BSM-13	BSM-01	BSM-01	BSM-01	BSM-01	BSM-25	BSM-25	BSM-25	BSM-25	BSM-25	BSM-25	BSM-35A	BSM-35A	BSM-35A	BSM-35A	BSM-35A	BSM-35A
Analysis	3	5	6	1	2	3	4	1	2	3	4	5	6	1	2	3	4	5	6
SiO_2	42.40	42.12	42.38	43.22	42.09	43.45	42.72	43.15	44.18	44.42	45.67	44.21	44.92	44.31	44.38	43.91	46.91	43.81	42.35
TiO_2	0.95	0.87	0.79	1.07	1.04	0.78	1.09	0.81	1.09	1.25	1.23	1.11	1.19	1.05	1.00	1.05	0.99	1.03	0.78
Al_2O_3	11.31	11.63	11.67	10.22	11.12	10.88	10.72	9.52	8.92	9.05	8.66	9.29	8.63	9.92	9.32	9.34	8.71	9.90	9.77
FeO	17.52	17.58	17.68	18.34	18.85	17.56	18.07	16.74	17.22	17.03	16.42	17.37	16.30	15.79	16.10	16.02	15.81	16.20	16.97
MnO	0.50	0.50	0.49	0.60	0.60	0.70	0.60	0.79	0.74	0.76	0.74	0.76	0.75	0.53	0.53	0.50	0.50	0.49	0.45
MgO	9.98	9.93	9.94	9.71	9.04	10.39	9.50	11.23	11.33	11.37	12.03	11.47	11.96	10.65	11.35	10.95	12.03	10.84	10.92
CaO	11.55	11.43	11.66	11.74	11.69	11.63	11.55	11.48	11.69	11.51	11.59	11.55	11.38	11.63	11.77	11.86	11.91	11.45	11.67
Na_2O	1.52	1.58	1.42	1.20	1.32	1.16	1.12	1.39	1.13	1.39	1.52	1.29	1.38	1.23	1.16	1.29	1.23	1.59	1.28
K_2O	0.77	0.87	0.81	0.99	1.19	0.81	0.98	0.86	0.89	0.97	0.89	0.92	0.84	0.92	0.90	1.03	0.88	1.03	1.03
Total	96.91	96.94	97.43	98.04	98.85	97.82	97.33	95.48	97.58	98.04	99.17	98.31	97.77	94.58	94.58	94.58	94.58	94.58	94.58
Si	6.377	6.359	6.336	6.501	6.380	6.450	6.459	6.536	6.607	6.608	6.698	6.557	6.671	6.688	6.663	6.665	6.833	6.615	6.483
Al iv	1.623	1.641	1.664	1.499	1.620	1.550	1.541	1.464	1.393	1.392	1.302	1.443	1.329	1.312	1.337	1.335	1.167	1.385	1.517
Al vi	0.382	0.401	0.398	0.312	0.366	0.353	0.369	0.235	0.180	0.194	0.195	0.180	0.181	0.453	0.311	0.336	0.328	0.377	0.245
Ti	0.108	0.105	0.099	0.121	0.119	0.087	0.124	0.093	0.123	0.140	0.135	0.124	0.133	0.119	0.113	0.120	0.108	0.117	0.090
Cr	0.003	0.000	0.000	0.002	0.000	0.000	0.000	0.000	0.005	0.004	0.000	0.000	0.000	0.006	0.002	0.002	0.007	0.004	0.016
Fe^{3+}	0.707	0.796	0.756	0.618	0.602	0.836	0.664	0.744	0.719	0.663	0.595	0.802	0.705	0.316	0.502	0.321	0.387	0.400	0.668
Fe^{2+}	1.497	1.384	1.455	1.689	1.788	1.343	1.621	1.293	1.355	1.381	1.352	1.263	1.241	1.640	1.464	1.677	1.496	1.601	1.430
Mn	0.065	0.069	0.065	0.080	0.082	0.082	0.081	0.101	0.093	0.095	0.092	0.096	0.094	0.068	0.067	0.065	0.062	0.062	0.059
Mg	2.238	2.246	2.227	2.178	2.043	2.299	2.141	2.535	2.526	2.522	2.631	2.536	2.647	2.397	2.540	2.479	2.612	2.439	2.492
Ca	1.861	1.834	1.842	1.892	1.899	1.850	1.871	1.863	1.874	1.834	1.821	1.835	1.811	1.881	1.893	1.928	1.859	1.853	1.915
Na	0.444	0.387	0.460	0.350	0.387	0.333	0.329	0.407	0.328	0.400	0.433	0.371	0.398	0.360	0.337	0.381	0.348	0.467	0.378
K	0.149	0.180	0.168	0.190	0.230	0.154	0.191	0.167	0.170	0.184	0.166	0.174	0.159	0.177	0.172	0.199	0.164	0.198	0.201
Total	15.454	15.400	15.470	15.432	15.515	15.337	15.390	15.437	15.371	15.418	15.421	15.379	15.367	15.418	15.403	15.508	15.371	15.518	15.494
Na (B)	0.139	0.166	0.158	0.108	0.101	0.150	0.129	0.137	0.126	0.166	0.179	0.165	0.189	0.119	0.107	0.072	0.141	0.147	0.085
(Na+K) (A)	0.454	0.400	0.470	0.432	0.515	0.337	0.390	0.437	0.371	0.418	0.421	0.379	0.367	0.418	0.403	0.508	0.371	0.518	0.494
$Mg/(Mg+Fe^2)$	0.599	0.619	0.605	0.563	0.533	0.631	0.569	0.662	0.651	0.646	0.661	0.667	0.681	0.594	0.634	0.596	0.636	0.604	0.635
$Fe^3/(Fe^3+Alvi)$	0.649	0.665	0.655	0.665	0.622	0.703	0.643	0.760	0.800	0.774	0.753	0.816	0.796	0.411	0.617	0.488	0.541	0.515	0.731
Sum of S^2	13	13	13	13	13	13	13	13	13	13	13	13	13	13	13	13	13	13	13
P (Kb)	6.5	6.8	6.8	5.6	6.4	6.0	6.1	5.1	4.5	4.5	4.1	4.7	4.2	5.4	4.8	4.9	4.1	5.4	5.4

TABLE I | **Continued**

	Santa Marta Batholith				Parashi Stock								
Sample	BSM-35A	BSM-35A	BSM-35A	BSM-35A	CM-3-2	CM-3-2	CM-3-2	CM-3-2	CM-3-2	CM-3-2	CM-4-16	CM-4-16	CM-4-16
Analysis	6	7	8	9	1	2	3	4	5	6	1	2	3
SiO_2	42.35	42.53	47.52	43.25	48.24	47.68	48.00	48.21	48.11	48.43	49.36	49.23	48.68
TiO_2	0.78	1.15	1.04	1.89	0.99	1.04	1.01	0.82	0.97	0.84	1.28	1.00	1.07
Al_2O_3	9.77	10.79	9.28	10.52	6.59	7.04	6.71	6.46	6.65	6.69	6.32	5.98	5.98
FeO	16.97	15.89	15.61	15.95	13.62	13.13	13.68	13.31	13.42	13.09	11.15	11.31	12.51
MnO	0.45	0.53	0.51	0.52	0.85	0.84	0.86	0.87	0.85	0.85	0.50	0.62	0.87
MgO	10.92	11.95	12.64	8.88	14.17	14.05	14.01	14.10	13.99	14.09	16.08	16.04	14.98
CaO	11.67	11.60	11.61	11.03	12.00	11.91	12.12	12.11	12.09	12.22	11.09	11.04	11.23
Na_2O	1.28	1.22	1.22	1.38	1.00	1.10	1.06	1.03	1.01	1.01	1.42	1.40	1.27
K_2O	1.03	0.91	0.83	1.01	0.55	0.50	0.52	0.44	0.51	0.50	0.36	0.32	0.34
Total	94.58	94.58	94.58	94.58	98.00	97.28	97.97	97.33	97.59	97.72	97.56	96.94	96.93
Si	6.483	6.354	6.778	6.685	6.969	6.933	6.953	7.016	6.990	7.021	7.014	7.039	7.026
Al iv	1.517	1.646	1.222	1.315	1.031	1.067	1.047	0.984	1.010	0.979	0.986	0.961	0.974
Al vi	0.245	0.254	0.339	0.603	0.091	0.138	0.099	0.123	0.129	0.164	0.072	0.046	0.044
Ti	0.090	0.129	0.112	0.220	0.107	0.114	0.110	0.090	0.106	0.092	0.137	0.107	0.116
Cr	0.016	0.003	0.006	0.001	0.002	0.003	0.000	0.001	0.000	0.004	0.000	0.000	0.000
Fe^{3+}	0.668	0.892	0.614	0.002	0.627	0.586	0.571	0.533	0.527	0.454	0.806	0.873	0.805
Fe^{2+}	1.430	0.993	1.179	2.060	1.019	1.010	1.087	1.088	1.103	1.133	0.520	0.479	0.704
Mn	0.059	0.066	0.062	0.069	0.103	0.104	0.105	0.107	0.104	0.104	0.060	0.076	0.106
Mg	2.492	2.662	2.687	2.045	3.051	3.045	3.025	3.058	3.029	3.045	3.406	3.419	3.224
Ca	1.915	1.857	1.775	1.827	0.000	0.000	0.002	0.000	0.002	0.003	1.689	1.691	1.737
Na	0.378	0.353	0.337	0.415	1.857	1.855	1.881	1.888	1.882	1.898	0.393	0.389	0.355
K	0.201	0.173	0.152	0.200	0.280	0.311	0.298	0.290	0.284	0.284	0.066	0.058	0.063
Total	15.494	15.382	15.264	15.442	0.102	0.092	0.096	0.081	0.094	0.092	15.147	15.137	15.155
Na (B)	0.085	0.143	0.225	0.173	0.143	0.145	0.119	0.112	0.118	0.102	0.311	0.309	0.263
(Na+K) (A)	0.494	0.382	0.264	0.442	0.239	0.258	0.275	0.259	0.260	0.275	0.147	0.137	0.155
$Mg/(Mg+Fe^2)$	0.635	0.728	0.695	0.498	0.750	0.751	0.736	0.738	0.733	0.729	0.868	0.877	0.821
$Fe^3/(Fe^3+Alvi)$	0.731	0.778	0.644	0.004	0.874	0.809	0.852	0.812	0.804	0.734	0.918	0.950	0.948
Sum of S^2	13	13	13	13	13	13	13	13	13	13	13	13	13
P (Kb)	5.4	6.0	4.4	6.1	2.3	2.7	2.4	2.3	2.4	2.4	2.0	1.8	1.8